Reformulation of Coal-Derived Transportation Fuels: Selective Oxidation of Carbon Monoxide on Metal Foam Catalysts

Annual Report

Reporting Period Start Date: September 25, 2001

Reporting Period End Date: December 31, 2002

Principal Authors: NC State: Mr. Paul Chin
Dr. Xiaolei Sun
Professor George W. Roberts
Professor James J. Spivey

Clemson: Mr. Amornmart Sirijarhuphan
Dr. James G. Goodwin, Jr.
Dr. Richard W. Rice

Date Report Issued: December 31, 2002

DOE Award Number: DE-FG26-O1NT41277

North Carolina State University
Department of Chemical Engineering
Box 7905
Raleigh, NC 27695-7905

Clemson University
Department of Chemical Engineering
Clemson, SC 29634-0909

Porvair Advanced Materials
700 Shepherd Street
Hendersonville, NC 28792

Disclaimer:

Abstract

Several different catalytic reactions must be carried out in order to convert hydrocarbons (or alcohols) into hydrogen for use as a fuel for polyelectrolyte membrane (PEM) fuel cells. Each reaction in the fuel-processing sequence has a different set of characteristics, which influences the type of catalyst support that should be used for that particular reaction. A wide range of supports are being evaluated for the various reactions in the fuel-processing scheme, including porous and non-porous particles, ceramic and metal straight-channel monoliths, and ceramic and metal monolithic foams. These different types of support have distinctly different transport characteristics. The best choice of support for a given reaction will depend on the design constraints for the system, e.g., allowable pressure drop, and on the characteristics of the reaction for which the catalyst is being designed. Three of the most important reaction characteristics are the intrinsic reaction rate, the exothermicity/endothermicity of the reaction, and the nature of the reaction network, e.g., whether more than one reaction takes place and, in the case of multiple reactions, the configuration of the network. Isotopic transient kinetic analysis was used to study the surface intermediates.

The preferential oxidation of low concentrations of carbon monoxide in the presence of high concentrations of hydrogen (PROX) is an important final step in most fuel processor designs. Data on the behavior of straight-channel monoliths and foam monolith supports will be presented to illustrate some of the factors involved in choosing a support for this reaction.

Table of Contents

List of Graphical Materials

List of Tables: Page

List of Figures:

1. Introduction

1.1 Preferential Oxidation

The development of practical fuel cell power for automotive transportation and for stationary applications will require the development of fuel processors that convert liquid fuels into hydrogen and carbon dioxide. These fuel processors will contain compact catalytic reactors that carry out a number of reactions between the fuel, oxygen, and steam: partial oxidation, steam reforming, water-gas shift, and selective oxidation of CO in the final hydrogen stream. Fuel processors must be compact, mechanically durable, quick-starting, responsive to transient demands, and inexpensive.

The gas stream that is fed to the fuel cell must have a very low (<10 ppm) concentration of CO to avoid poisoning the fuel cell electrode [**11,12**]. The final selective oxidation step requires a catalyst that is active for the oxidation of CO (Reaction 1) in order to reduce the concentration of CO from about 1% to less than 10 ppm in the presence of high concentrations of H_2, CO_2, steam, using a minimum volume of catalyst.

$$CO + \frac{1}{2}O_2 \rightarrow CO_2 \qquad (1)$$

However, the catalyst must not oxidize a significant quantity of hydrogen (Reaction 2)

$$H_2 + \frac{1}{2}O_2 \rightarrow H_2O \qquad (2)$$

$$CO + H_2O \leftrightarrow H_2 + CO_2 \qquad (3)$$

since H_2 is the fuel used at the anode of the fuel cell, nor should it have a strong preference to the water-gas-shift reaction (Reaction 3). Hydrogen that is consumed by Reaction 2 during the selective oxidation step must be replaced by increasing the size of the fuel processor, and increasing the rate of feed to the fuel processor. Therefore, the catalyst not only must be highly active for the oxidation of CO, it also must be highly selective for Reaction 1 over Reaction 2. The process described above is known as "preferential oxidation" in the fuel cell community, and is often referred to using the acronym "PROX".

Because of the exothermic nature of these two oxidation reactions, some commercial designs for this element of the fuel processor are based on two adiabatic reactors in series, with an intermediate cooling step [**13**].

Packed catalyst beds, as well as ceramic monoliths, have been evaluated for the PROX reactor. Other potential supports include metal monoliths. The objective of this research is to demonstrate that effective PROX catalysts could be prepared on metallic foam supports, and to compare these catalysts with identical catalysts prepared on ceramic monoliths.

1.2 Literature Review

The selective oxidation of CO in the presence of hydrogen was first studied using a Pt/alumina catalyst in 1963. In 1997, Igarashi et al. investigated the effect of the support on the selectivity of Pt catalysts for CO oxidation and found that Pt supported on mordenite showed the highest selectivity, as well as high conversion of CO during oxidation at low oxygen concentration [**13**]. In the same year, Kahlich et al. [**14**] used the preferential oxidation process (PROX) to determine the optimum temperature, the reaction order, and the apparent activation energy of CO oxidation on Pt/Al_2O_3. It was found that the optimum temperature was 200^oC at 1 bar and the reaction orders were -0.4 for CO and +0.8 for O_2 for temperatures between 150^oC and 250^oC.

Korotkikh and Farrauto [**1**] investigated the effect of a promoter oxide on the activity of 5 wt% Pt/alumina. With a base metal oxide promoter, the CO conversion was significantly increased from 13.2 to 68% at 90^oC and a molar ratio of $O_2/CO = 0.5$ without affecting the selectivity. Recently, Manasilp and Gulari [**9**] studied the selectivity of a 2% Pt/alumina sol-gel catalyst in a mixed feed stream including CO_2 and water. This catalyst was found to have an activity and a selectivity high enough to oxidize CO in hydrogen down to a few ppm. Water vapor had a positive effect in reducing the activation energy, resulting in an increase in conversion without any significant change in selectivity. Carbon dioxide in the feed stream decreased the activity of the catalyst in the absence of water vapor. Other metal-based catalysts have also been found to be active for selective CO oxidation, including Ru [**4**], Rh [**4**], and Au [**16-18**].

Most of the previous studies of the selective oxidation of CO have been conducted under steady-state conditions. However, although Nibbelke et al. [**19**] commented in their paper that $Pt/\gamma\text{-}Al_2O_3$ exhibited a higher initial activity during startup compared to the activity measured after a few hours on stream, initial catalyst deactivation has not been investigated. This initial rapid deactivation can result in a loss of 90% of the initial activity of a Pt catalyst before steady state is reached.

In order to obtain surface kinetic information about CO oxidation, isotopic-transient kinetic analysis (ITKA) has been used in a portion of this study. Since it allows in-situ measurement of the concentration of surface intermediates and their intrinsic reactivities while the reaction is maintained at stable reaction conditions, SSITKA (steady-state isotopic-transient kinetic analysis) or ITKA(when not at steady state) is one of the most powerful techniques for the kinetic study of heterogeneous catalysis. Extensive details about the use of (SS)ITKA are given in references [**20,21**]. A conventional selective CO oxidation catalyst, 5% Pt/Al_2O_3 was employed, and the effect of time-on-stream on CO oxidation rate, selectivity, concentration of surface intermediates, and catalyst intrinsic activity was investigated. Since this catalyst possesses very high activity and selectivity during initial reaction, a better understanding of the deactivation phenomena could lead to strategies to prevent or slow down deactivation, resulting in a better catalyst design.

1.3 Metal Foam Catalyst Supports

Metallic foams consist of irregular, open cells in a rigid matrix, as shown in Figure A1a in Appendix A. The active catalytic material is added to the foam via a washcoating process, which is described in more detail later. Foams have been used as catalyst supports in several applications, such as radiant burners and exhaust catalysts for small engines. Among the metals of interest, Fecralloy® was particularly suited for the present study. The composition of Fecralloy® is: 72.8% Fe/ 22% Cr/ 5% Al/ 0.1% Y/ 0.1% Zr.

Metal foams have several potential advantages for fuel processors:

(1) The porosity of the foam can be very high, which helps to minimize pressure drop and results in a low heat capacity, which provides a rapid response to transients and to changes in the operating conditions of the fuel processor;

(2) Metal foams can be formed in shapes other than right cylinders and square blocks, as shown in Figure A1b in Appendix A, allowing the fuel processor to fit the demanding space requirements of an automotive fuel processor, which may not have a straight flow path. These foams have already been shown to be useful in similar situations, e.g., exhaust catalysts for small engines such as lawn mowers and power saws, where straight-channel monoliths could not be used;

(3) The cell density is variable over a larger range than metallic monoliths. Specifically, metallic foams can be made with densities as low as 3% of the theoretical volume (i.e. void volume of 97%). This allows the inevitable trade-off between pressure drop and mass transfer rates to be optimized for the wide range of flow rates required in an automotive fuel processor;

(4) The foams can be metallurgically bonded to reactor shells, forming light-weight, durable, and rugged reactors;

(5) Metal tubes can be mechanically inserted into the foam structure during the manufacturing process, as shown in Figure A1c in Appendix A. These tubes can be used to transfer heat out of the PROX catalyst. This type of heat transfer could, in principle, eliminate the need for a two-stage CO oxidation unit, saving space and cost, and minimizing hydrogen oxidation.

(6) The cellular nature of the metallic foams permits radial and axial flow and mixing of fluid. This type of mixing can help to alleviate problems associated with misdistribution of the gas that is fed to the reactor.

During this research, a Pt/Al_2O_3 catalyst promoted with Fe was evaluated. This catalyst was supported on a series of metallic foams with varying porosity and pore size. As a control, the same catalyst, deposited on a conventional ceramic monolith, was evaluated. Finally, a metal monolith and a ceramic foam were evaluated briefly. These supports were compared at the same volumetric washcoat loading and catalyst composition.

2. Executive Summary

This project is a joint effort among NC State University, Clemson University, and Porvair Fuel Cell Technologies (PFCT, Hendersonville, NC).

Several different catalytic reactions must be carried out in order to convert hydrocarbon fuels or oxygenates into hydrogen for use as a fuel for proton exchange membrane (PEM) fuel cells. Typically three sequential reactions are used: autothermal reforming, water-gas-shift, and preferential oxidation (PROX). In this last reaction, CO is selectively oxidized in the presence of ~40% hydrogen to prevent poisoning of the fuel cell electrode.

This paper focuses on the use of metal foams as supports for PROX catalysts. Ceramic and metallic straight-channel monoliths, conventional packed beds, and ceramic foams are candidate supports for these catalysts. The high thermal conductivity, mechanical strength, and wide range of physical properties of metal foams suggest that they may be suitable for this application. Here, these foams are compared directly with straight-channel ceramic monoliths for the PROX reaction.

Metal foams with void volumes of 96% and 88% were prepared by PFCT from Fecralloy®, a ferric alloy with an empirical composition of Fe 72.8/Cr 22/Al 5/Y 0.1/Zr 0.1. These foams were washcoated and impregnated with 5%Pt-0.5% Fe [**2,3**]. Ceramic straight-channel monoliths were prepared with nominally identical volumetric loadings of catalyst (1.6 g cat/in^3) by similar washcoating techniques. The catalysts were calcined at 300°C for 2 h and tested in an adiabatic fixed bed reactor. Outlet CO and oxygen concentrations were measured continuously using an NDIR analyzer. CO selectivity is calculated as $[0.5 * (CO_{in} - CO_{out})/(O_{2,in} - O_{2,out})]$.

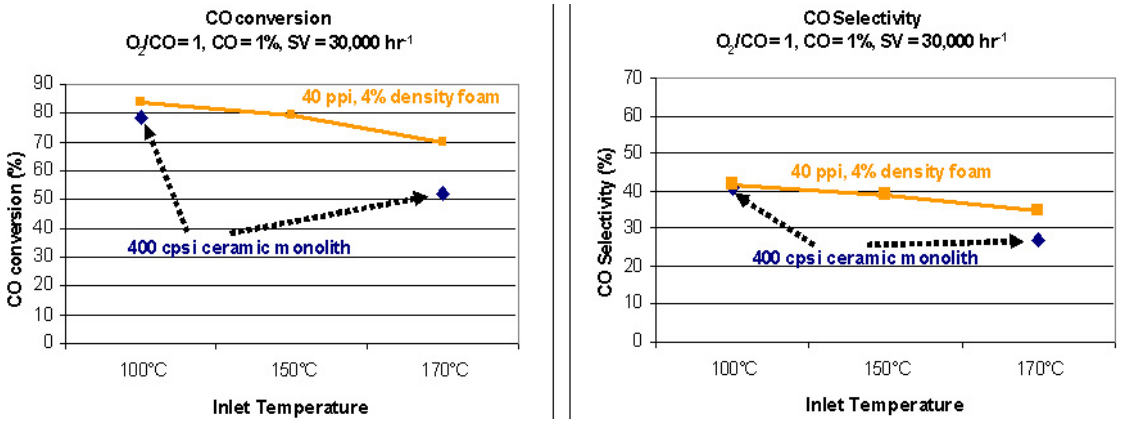

Fig. 1. Comparison of CO conversion and selectivity on metal foams and straight-channel ceramic monoliths

Figure 1 shows that the CO conversion and CO selectivity (the proportion of CO oxidized to CO_2 to the ratio of H_2 oxidized) for catalysts on a metal foam and a ceramic monolith are comparable when tested under the same operating conditions: P = 2 atm (abs.); inlet

gas composition = H_2 – 42%, CO_2 – 9%, H_2O – 12%, CO – 1.0%, O2 – 0.25-1.0%, and N_2 – Balance; inlet temperature = 80-170°C; space velocity = 5,000-60,000 hr^{-1}, catalyst length = 2"-6".

Equilibrium calculations suggest that the decrease in CO conversion with increasing temperature is consistent with an increase in the equilibrium concentration of CO formed by the reverse water-gas-shift reaction. The decrease in CO selectivity is consistent with an increase in the rate of hydrogen oxidation compared to CO oxidation at higher temperatures on Pt-base metal catalysts [**2**]. Figure 2 shows that catalyst performance is very sensitive to iron loading. It has been suggested that Fe activates oxygen at the relatively low temperatures of this reaction in a dual-site mechanism [**2**]. Testing of 0%-1% wt. loadings of iron on a 5% Pt catalyst shows that this promoting effect is significant, and begins at an Fe loading of ~0.5 wt%.

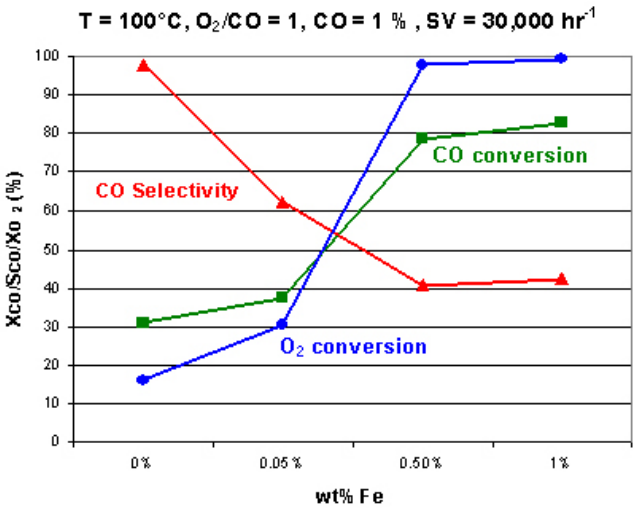

Fig. 2. Effect of Fe loading on a 5% Pt PROX catalyst

The selective oxidation of CO in the presence of hydrogen using 5% Pt/γ-Al_2O_3 exhibited high initial partial deactivation before reaching steady state. The observed rate and CO_2 selectivity were very high during the initial reaction period, but decreased significantly with time-on-stream. By using isotopic transient analysis, the pseudo-first-order intrinsic rate constant was found to be relatively constant compared to the concentration of surface CO_2 reaction intermediates. It can be concluded that the deactivation of this Pt catalyst is mainly the result of a decrease in the concentration of surface intermediates, not the intrinsic activity. In addition, regeneration of the catalyst in the stream of hydrogen at temperatures higher than or equal to 300°C can completely recover the initial activity and selectivity of the deactivated catalyst. Approximately 12% of surface Pt was likely covered with carbonaceous species during initial deactivation. From this result, we suggest that the deactivation of Pt is due to carbon deposition on the Pt surface and that this carbon deposition also caused a significant decrease in CO_2 selectivity. Possibly CO_2 selectivity is decreased because CO adsorption is affected more than H_2 and O_2 adsorption.

3. Experimental

3.1 Catalyst Preparation (Metal Foams, Ceramic Monoliths, Provided by PFCT)

1" inner diameter (ID) and 2" length metallic foams and monolith supports were provided by Porvair Fuel Cell Technology (PFCT), in Hendersonville, NC. A series of Fe promoted Pt catalysts were synthesized and washcoated onto these supports, with a washcoat loading of approximately 1.6 g cat/in^3.

The four different supports were included in our tests: four metal foams, which possessed 40 ppi (pores per inch), 4% density; 40 ppi, 12% density; 20 ppi, 4% density; and 20 ppi, 12% density structure; one 400 cpsi (cells per square inch) ceramic straight - channel monolith; one 20 ppi, 11% ceramic foam; one corrugated metal monolith. The metal monolith was made of a spiral-wound corrugated metal support with a repeating pattern of ~3 mm. This results in an open face are roughly equivalent to the 400 cpsi ceramic straight-channel monolith.

Pores per inch (ppi) can be described as the number of pores in the foam per given inch. For example, a 20 ppi foam will have larger channel sizes compared to a 40 ppi foam. A 40 ppi foam would give greater tortuosity compared to a 20 ppi foam. Secondly, percent density can be described as the actual volume of foam taken up divided by the total volume of the foam. For example, a 4% density foam has 96% void volume, while a 12% density foam has a 88% void volume. Finally, cells per square inch (cpsi) can be similarly characterized by the number of cells per given inch. For example, a 400 cpsi straight-channel monolith has smaller channels than a 200 cpsi straight-channel monolith. Figure A2 in Appendix A gives an example.

3.2 Catalyst Preparation (NCSU)

Kyle Bishop, a summer student from the University of Virginia, in the Green Processing research experience for undergraduates (REU) program, prepared powder samples to be used for washcoating of blank metal foams supplied by PFCT. These powders were not used in washcoating of the foam samples reported here, but will be used in later work. The technique is outlined below.

<u>Pt catalyst</u>:

1. Start with γ-Al_2O_3 powder with a particle size ranging from 63-200μm. Determine the pore volume to mass ratio by impregnating to incipient wetness with deionized water.

2. Calculate the appropriate concentration of hydrogen hexachloroplatinate (IV) hexahydrate ($H_2Cl_6Pt{\cdot}6H_2O$) solution to achieve the desired platinum loading. Impregnate to incipient wetness (i.e. the powder begins to look wet or shiny).

3. Dry in a 110^oC oven for 12 hr to remove all water.

4. Calcine in air at 450^oC for 5 hr.

Fe-promoted Pt catalysts:

1. Start with Pt/γ-Al_2O_3 powder. Determine the pore volume to mass ratio by impregnating to incipient wetness with deionized water. (Note: The ratio may or may not be less than the pure alumina depending on the platinum loading.)

2. Calculate the appropriate concentration of iron (III) nitrate nonahydrate ($Fe(NO_3)_3 \cdot 9H_2O$) to achieve the desired iron loading. Impregnate the Pt/γ-Al_2O_3 powder to incipient wetness.

3. Dry in a 110^{o}C oven for 12 hr to remove all water.

4. Calcine in air at 300^{o}C for 2-3 hr.

Ni-promoted Pt catalysts:
Prepare exactly as the iron-promoted catalysts using nickel (II) nitrate hexahydrate ($Ni(NO_3)_2 \cdot 6H_2O$) as the nickel precursor.

3.3 Catalyst Preparation (Clemson)

A catalyst consisting of 5 wt% Pt on γ-Al_2O_3 powder was prepared by incipient wetness impregnation. The support (Al_2O_3, Vista B) was first calcined at 500^{o}C for 10 h before being impregnated at room temperature with an aqueous solution of chloroplatinic acid hexahydrate. The catalyst was then dried overnight at 110^{o}C and calcined at 500^{o}C for 2 h under flowing dry air.

3.4 Reactor system (NCSU)

Figure A3 in Appendix A shows a schematic of the process design used for this study. Gases were fed from four cylinders, which contain 10% CO/balance N_2, 10% O_2/balance N_2, 17.6% CO_2/balance H_2 and ultra high pure (UHP) N_2, respectively. Four mass flow controllers were used to measure and control the gas flow rate from each cylinder. A carbonyl trap (activated carbon bed) was installed to remove any iron and/or nickel carbonyls that might be present in the 10% CO/N_2 line. An oxygen trap was installed on the 17.6% CO/H_2 line to remove any traces of O_2. Liquid water, which was supplied to the system by a HPLC pump, was then added to the gas stream. This mixture then passed through a fluidized sand bath to generate steam and to heat up the gas stream to the desired temperature.

Foam and monolith support catalysts were wrapped with ceramic fiber insulation and fitted into a 1 1/8" ID stainless steel reactor. The reactor design is shown in Figure A4 in Appendix A. Trying to maintain an adiabatic operation, the reactor was first wrapped with a ceramic blanket as isolation layer, and secondly with heating tapes, providing a temperature close to the inner reactor temperature. Lastly, another insulation layer was placed around the reactor. This design minimized the heat loss through the reactor.

A control thermocouple was positioned at the inlet section of the catalyst support, and another thermocouple was positioned at the outlet section of the catalyst bed. With the two thermocouples, the temperature rise (ΔT_{ad}) was recorded to monitor the reactor

operation. A back pressure regulator downstream of the reactor kept the pressure in the reactor at 2 atm (absolute).

After passing through the reactor tube, a certain amount of the gas outlet stream passed a gas sample conditioning system, or a gas chiller system, which was installed prior to the gas analyzers. The rest of the gas outlet stream branched off to a room-temperature partial condenser, where most of the water was removed before venting to the atmosphere. This gas conditioning system is a two channel, thermoelectric heat exchanger. It has a chill capacity to 5°C dew point moisture. After the gas conditioning system, this certain amount dry gases then was introduced into CO and O_2 analyzers. A wet test meter was installed prior to the analyzers to allow us to check the flow rate, and served as a vent.

For the gas product, CO was measured using an on-line NDIR (nondispersive infrared) gas analyzer, while O_2 was measured with a paramagnetic analyzer. Both analyzers were purchased by California Analytical Instruments, Inc. The specially designed CAI model 300 analyzer includes two CO analyzers and one O_2 analyzer. The high concentration CO analyzer had two ranges, which allowed it to measure CO concentrations from 0-3000 ppm or 0-1.5%. The low concentration CO analyzer contained two ranges as well, 0-200 ppm or 0 - 1000 ppm. The paramagnetic O_2 analyzer has 3 ranges, 0 – 1%, 0 – 15% or 0 – 25%. By choosing a suitable range, the CO/O_2 analyzer was able to provide an accurate reading.

3.5 Reaction System (Clemson)

The system consisted of a differential flow reactor connected to a gas chromatograph and mass spectrometer, as shown in Figure 1 in Appendix B. The catalyst was placed in a 0.3 in. (7.6 mm) I.D. stainless steel reactor. The pressure in the reactor was kept constant at 1.8 atm using a back pressure regulator. A thermocouple was placed at the bottom of the catalyst bed. A Valco two-position valve with an electric actuator was used to switch between the labeled CO (^{12}CO vs. ^{13}CO). The reactor outlet was connected to a gas chromatograph (Varian CP-3380) and a quadrupole mass spectrometer (Pfeiffer Vacuum). The reaction effluent was partially induced into the mass spectrometer via a 1/16 inch capillary tube and a differential pumping. A 6-port sampling valve was placed between the reactor outlet and the GC. In the GC, the products were separated by a 6-ft long 80/100 mesh carbosphere column (Alltech). Hydrogen, carbon monoxide, and oxygen were first separated at 35^{o}C and then the GC was ramped to 150^{o}C at 20^{o}C/min to determine the concentration of CO_2.

3.6 Testing Conditions (NCSU)

The catalyst was evaluated at the following gas compositions: H_2 - 42%, CO_2 – 9%, H_2O – 12%, CO – X%, O_2 – Y%, and N_2 – balance gas. This composition simulated the reformulated gas stream exiting the WGS reactor. A wide range of testing conditions had been evaluated, with a fixed reactor pressure of 2 atm (abs.). The inlet temperature was varied from 80°C to 170°C. The O_2/CO ratios were tested from 0.25 – 1.0. Space velocity was studied in a range of 5,000 hr^{-1} to 60, 000 hr^{-1}. Linear velocity was altered

from 21.3 cm/sec to 64.0 cm/sec. The performance of the catalysts was studied with respect to the aforementioned testing conditions. The CO conversion, CO selectivity and O_2 conversion were examined as a measure of the catalyst performance.

The effect of reverse water-gas-shift (rWGS) reaction also was studied. This was achieved by cutting off the CO inlet while keeping all the other operating conditions the same. Under this circumstance, the CO measured by the NDIR in the product gas stream was formed only through the rWGS reaction. This rWGS reaction study revealed the actual limiting conditions for the CO conversion with our catalyst formula and testing conditions.

3.7 Reaction Measurements (Clemson)

The catalytic activity of the catalyst for the selective oxidation of CO in the presence of hydrogen was determined at 90°C and 1.8 atm. Prior to CO oxidation, approximately 50 mg of catalyst was diluted with α-alumina and reduced in a stream of hydrogen at 550°C for 1 h. After reduction, the temperature was gradually decreased over 4 h to the reaction temperature, at which time the flow was switched to a feed stream containing 45% H_2, 53% He, 1% CO and 1% O_2. A gas space velocity of ~190,000 h^{-1} was used. The CO conversion and selectivity were determined periodically until the reaction reached steady state.

Because of the detection limitation of the thermal conductivity detector (TCD) at low concentrations of CO_2, the amount of CO_2 produced during reaction was calculated from the amount of CO consumption. However, at high conversions of CO up to 50%, the conversions calculated based on CO_2 and CO concentrations were the same within experimental error. Since the change in total gas volumetric flow rate during reaction was relatively small, CO conversion, O_2 conversion, and selectivity were calculated using

$$\%\text{CO conversion} = \left(1 - F_{CO} \Big/ F_{CO_0}\right) \times 100\% \approx \left(1 - C_{CO} \Big/ C_{CO_0}\right) \times 100\% \tag{4}$$

$$\%O_2 \text{ conversion} = \left(1 - F_{O_2} \Big/ F_{O_{20}}\right) \times 100\% \approx \left(1 - C_{O_2} \Big/ C_{O_{20}}\right) \times 100\% \tag{5}$$

and $$\%CO_2 \text{ selectivity} = 0.5 \times \frac{(F_{CO_0} - F_{CO})}{(F_{O_{20}} - F_{O_2})} \times 100\%$$

$$\approx 0.5 \times \frac{(C_{CO_0} - C_{CO})}{(C_{O_{20}} - C_{O_2})} \times 100\% \tag{6}$$

where F_i and F_{i0} are the molar flow rates of species *i* at the reactor outlet and inlet, respectively, and C_i and C_{i0} are the concentrations of species *i* at the reactor outlet and inlet, respectively.

3.8 Catalyst Characterization (Clemson)

The catalysts sample was characterized using the following techniques.

BET Surface Area

Measurement was performed to determine the total BET surface area of catalyst sample after calcination. Prior to the BET measurement, the catalyst sample was degassed at 300^{o}C for 3 h. The sample was then analyzed using N_2 adsorption at 77 K in a Micromeritics ASAP 2010.

X-ray Powder Diffraction

X-ray diffraction (XRD) was used to determine the bulk crystalline phase of the platinum catalyst after calcination. The XRD patterns were collected with a Phillips X'pert X-Ray diffractometer with monochromatized CuK_α radiation (λ=1.54439 Å). The sample was scanned at 1 degree/min in the range 2θ=2-90 degrees.

Hydrogen Chemisorption

Static hydrogen chemisorption at 35^{o}C on the reduced platinum catalyst was used to determine the concentration of reduced surface platinum atoms. Prior to H_2-chemisorption, the calcined catalyst was evacuated to 10^{-6} mmHg at 100^{o}C for 15 minutes and then reduced in flowing hydrogen at 550^{o}C for 2 h after ramping up the temperature at 10^{o}C/min. The catalyst was evacuated to 10^{-6} mmHg at 550^{o}C for 30 min to desorb any hydrogen before the temperature was lowered to 35^{o}C and evacuated for 30 min. The concentration of exposed metal atoms on the surface was calculated by extrapolating the irreversible adsorption isotherm to zero pressure and assuming the coverage of one H atom per Pt atom exposed on the surface. This measurement was performed in a Micromeritics ASAP 2010 using ASAP 2010C V 3.00 software.

3.9 Isotopic-Transient Kinetic Analysis (ITKA) (Clemson)

Isotopic transients were taken by switching between isotopically labeled CO (^{12}CO vs. ^{13}CO). A trace of argon was present in the ^{12}CO stream to measure the gas phase holdup in the reaction system. The kinetic parameters, such as average surface residence time and concentration of surface intermediates, were calculated using the method described by Shannon and Goodwin [**20**]. By integrating the normalized step-decay of step input response, the overall mean surface residence time of all adsorbed surface intermediates can be determined. The decrease in the transient response of the old label and the increase in the transient response of the new label in the CO_2 and CO exiting the reactor were monitored by a mass spectrometer equipped with a high-speed data acquisition system interfaced to a personal computer using Balzers Quadstar 422 v 6.0 software.

4. Results and Discussion

4.1 Catalyst Screening

It is well known that Pt based supported catalysts are active oxidation catalysts. On the other hand, CO also adsorbs very strongly on Pt [**1-3,8,9**]. The Pt surface must be covered with CO until the de-adsorption temperature of CO is reached, or the gas phase CO concentration approaches zero. CO oxidation is unlikely to happen with fully CO covered Pt surface since there is no active oxygen on the Pt surface. Kinetically, the reaction with CO and O_2 occurs with a Langmiur-Hinshelwood type of mechanism [**1**,**5**,**6**]. Making this mechanistic behavior assumption, it is necessary for both the O_2 and the CO to be adsorbed onto the Pt surface for a reaction to occur between the two gases. In order to use Pt as a catalyst, there must be another way for the O_2 to absorb and react.

Previous research has found that promotion with a base metal, such as Fe, Mn, Ni [**3**] as well as Sn [**10**], would minimize the inhibition and deactivation caused by the strong adsorption of CO on the Pt surface. Among all these promoters, Liu et al. [**2**] found that for Fe-oxide promoted Pt/alumina catalyst, Fe oxide provides the active oxygen for the CO oxidation. In their research, they believed that the only reaction possible for Pt/alumina is when adsorbed CO reacts with adsorbed O on adjacent Pt sites. Fe oxide in the promoted catalyst is located on or immediately adjacent to the surface of the Pt metal, therefore creating a non-competitive dual site adsorption pathway enhancing the CO activity for the promoted catalyst.

Because of this phenomenon, we initiated our research with 0.5 wt% Pt catalyst promoted with 0.005 wt% Fe. This catalyst formula was the most active of a series of materials studied by Straschil and Egbert [**3**]. The catalyst was washcoated onto a 1" ID and 2" length ceramic monolith.

This catalyst was placed on both metal foam and ceramic monolith. For an inlet CO concentration of 1.0%, both catalysts showed an O_2 conversion of less than 10%, which leads to a low CO conversion. In addition, there was no significant adiabatic temperature rise, even at an inlet temperature of 170^{o}C. The low overall O_2 conversion also indicated that the competitive hydrogen oxidation reaction was inhibiting the reaction. In order to test this point, the CO inlet gas was shut off, to allow only hydrogen oxidation. At inlet temperatures of 100^{o}C and 170^{o}C, O_2 conversion was close to 100%, and there was a ΔT_{ad} between 65-90^{o}C, significantly increasing the reactor outlet temperature. When the CO inlet line was reopened, the O_2 conversion dropped and the outlet concentration increased, while the outlet temperature quickly dropped back to the inlet temperature.

This strong CO poisoning phenomena suggested that the 0.005% Fe promoted on the 0.5% Pt catalyst acted as a pure Pt catalyst. Such a low Fe concentration did not provide enough active sites for the O_2 adsorption, and hence the CO oxidation reaction was stifled. A similar CO poison phenomenon has been observed [**1,4**].

Subsequently, a series of 5 wt% Pt coupled with a series of different Fe loadings, ranging from 0 wt% to 1.0 wt%, were synthesized onto ceramic monolith supports with 1" ID, 2"

length, and 400 cpsi. The CO conversion, CO selectivity, and O_2 conversion were measured on these catalysts:

$$\text{CO Conversion} = \frac{CO_{outlet} - CO_{inlet}}{CO_{inlet}} \quad (7)$$

$$\text{CO Selectivity} = \frac{1/2[CO_{outlet} - CO_{inlet}]}{O_{2,outlet} - O_{2,inlet}} \quad (8)$$

$$O_2 \text{ Conversion} = \frac{O_{2,\,outlet} - O_{2,inlet}}{O_{2,\,inlet}} \quad (9)$$

where CO is the CO concentration, and O_2 is the O_2 concentration.

At T_{in} = 170°C, all catalysts exhibited similar results. Figure 3, showed that the CO conversion, CO selectivity, and O_2 conversion are independent of Fe loading. This suggests that lower inlet temperatures were needed.

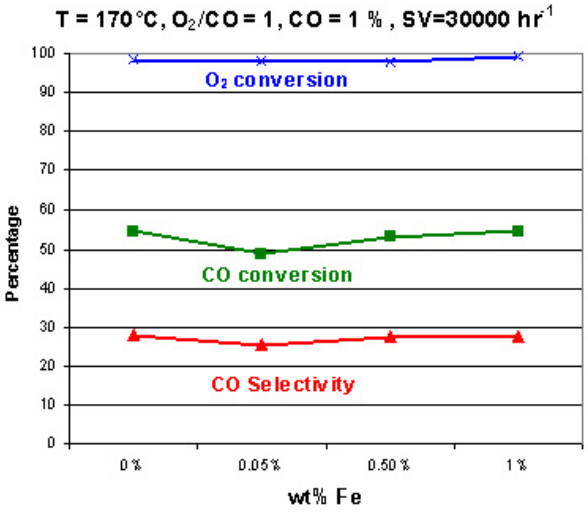

Fig. 3. Effect of Fe loading on a 5% Pt PROX

Figure 2 in the Executive Summary shows an example of catalyst performance at T_{in} = 100°C, CO inlet concentration = 1.0, O_2/CO ratio = 1.1, and a gas hourly space velocity (GHSV) = 30,000 hr^{-1}. At these conditions, there are very distinct differences in the conversions and selectivity. At low Fe loading (pure Pt catalyst, 0.05 wt% Fe), the catalysts gave low activity; the CO conversion was less than 40%, and the O_2 conversion was less than 30%. At higher Fe loadings (0.5 wt%, 1.0 wt% Fe), the activity of the catalysts increased significantly; the CO conversion was approximately 80%, and the O_2 conversion close to 100%.

Since the stoichiometric ratio of the O_2/CO reaction is 0.5, it is not possible to achieve a high CO selectivity with a large excess of oxygen. With an O_2/CO ratio = 1.0, the 0.5 wt% and 1.0 wt% Fe promoted catalysts achieved 40% and 42% CO selectivity, respectively.

4.2 Reverse Water-Gas-Shift (rWGS) Reaction

The decrease in CO conversion at higher temperatures suggests that CO is formed by the reverse water-gas-shift (rWGS) reaction. Experiments with no CO concentration in the inlet (shutting off the CO inlet line) were carried out to determine the adiabatic temperature rise (ΔT_{ad}) for these reactions. The theoretical ΔT_{ad} can be calculated as follows:

$$\Delta T_{ad} = \frac{-F_{A0} X * 2 * \Delta H^{o}_{RX}}{F_0 \sum_{i=1}^{n} \theta_i \hat{C}_{Pi}} \qquad (10)$$

Where F_{AO} is the flow rate of CO, F_0 is the total flow rate, X is the CO conversion, ΔH^{o}_{RX} is the heat of reaction, θ_i is the fractional composition of species i in the gas stream, and $\hat{C}_{pi}$ is the average heat capacity of species i in the gas stream.

The inlet feed gas stream for our reactor is modeled after the reformate gas stream in a PROX fuel cell. For reformate gas stream compositions (i.e. 40-75% H_2, 15-20% CO_2, ~10% H_2O, 0-35% N_2, and 0.5-1.0% CO), the rWGS reaction can severely limit the conversion of CO [**1,4,9**]. These limitations are more significant at higher temperature (i.e. > 170°C), where the oxidation catalyst is moderately active for the rWGS reaction:

$$H_2 + CO_2 \leftrightarrow H_2O + CO \qquad (11)$$

Korotkikh and Farrauto [**1**] carried out tests without CO_2 in the inlet gas in order to eliminate the possibility of forming CO by the rWGS reaction.

To test the activity of our catalysts for the rWGS reaction, CO was removed from the inlet stream. Therefore, any CO detected in the outlet stream can be attributed to the rWGS reaction. The equilibrium limitations were computed through a theoretical model, with the following assumptions:

1) All oxygen was consumed by the oxidation reactions (equations 1 and 2)
2) The ideal gas law (PV=nRT) was valid
3) The C_p's and ΔH_{rxn} are constant over our given range of temperatures

Figure 4 shows the measured outlet CO concentration, and the calculated CO concentration for the shift equilibrium, for a 5 wt% Pt, 0.5 wt% Fe catalyst. When there is no hydrogen oxidation present, the outlet CO concentration remains at a low value, around 158 ppm. As the inlet O_2 concentration increases, the outlet temperature is significantly increased, generating more CO in the outlet stream because of the temperature dependency in the rWGS reaction.

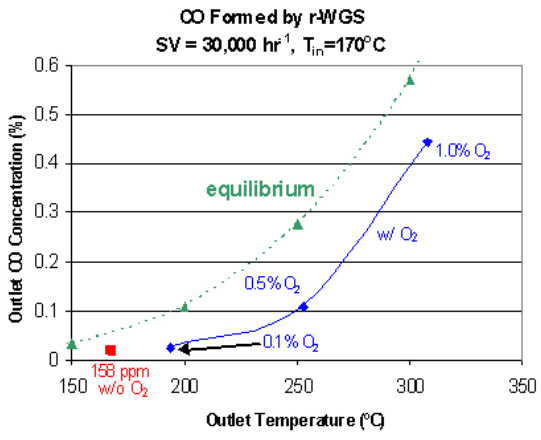

Fig. 4. rWGS reaction with and without the presence of O_2

Although the CO concentration is below the equilibrium value for the rWGS reaction, the trend with temperature follows the equilibrium. This equilibrium line gives us a limit to the minimum level of CO exiting the PROX reactor. Figure

A5 in Appendix A gives similar data for the CO outlet concentration for all the ceramic monolith data.

The Fe promoted 5 wt% Pt catalysts have the following activity order:

$$0.5 \text{ wt\% Fe} < 1.0 \text{ wt\% Fe} < 0.0 \text{ wt\% Fe} < 0.05 \text{ wt\% Fe}$$

No obvious relationship has been discovered between the iron loading and the shift reaction activity. Basted on these results, in addition to the catalyst performance study on the ceramic monoliths, we chose to use a 5 wt% Pt, 0.5 wt% Fe as the catalyst formulation for the metal foam support study.

4.3 Comparison of Metal Foam and Ceramic Monolith

4.3.1 Pt-Fe catalyst (No Pretreatment, Metal Foam)

A 5% Pt-0.5% Fe catalyst was washcoated on a series of metal foams with the same volumetric washcoat loading (1.6 g/in^3). The four different metal foams, all with 1" ID and 2" length, were 40 ppi 4% density, 40 ppi 12% density, 20 ppi 4% density, and 20 ppi 12% density. Figure 5 shows the CO conversion for these different metal foams.

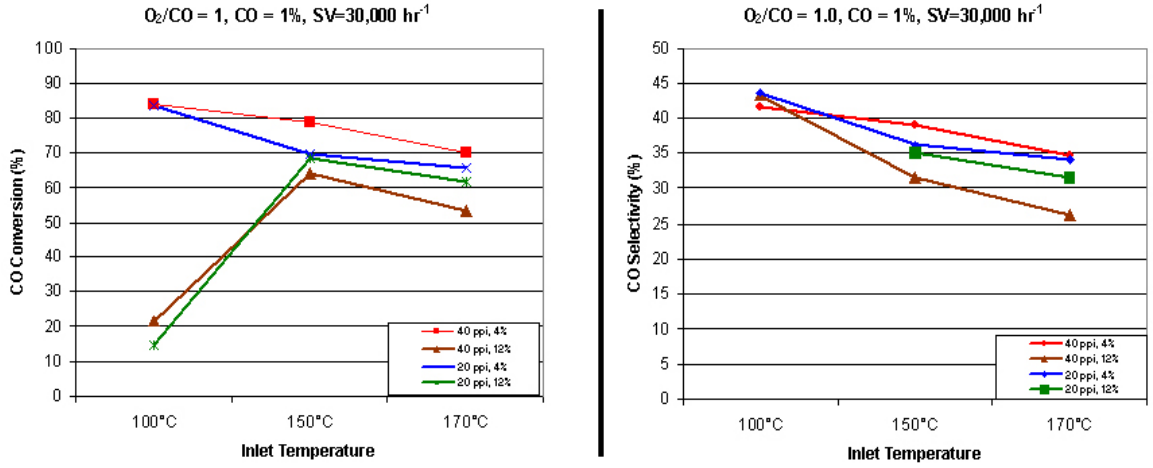

Fig. 5. CO conversion (left) and CO selectivity (right) for different types of metal foams

From the data, it can be seen that higher ppi, higher void volume (consequently lower density) has higher CO conversion and CO selectivity compared to their counterparts for all three inlet temperatures studied. O_2 conversion was nearly 100% for all cases, excluding the two lower conversions from the 12% density foams.

Note that at the T_{in} = 100^{o}C, you the 12% density foams have an extremely low CO conversion (< 22%). The order of activity for CO oxidation is:

20 ppi, 4% density < 20 ppi, 12% density < 40 ppi, 12% density < 40 ppi, 4% density

The higher the ppi, the more tortuous the flow path, allowing more mixing both axially and radially.

Increasing temperature results in decreasing CO conversion and CO selectivity. As the inlet temperature is increased, the probability of CO desorption from the Pt surface increases [**4,9**]. The CO desorption temperature from Pt is T~160°C [**9**]. Therefore, as temperature increases, CO desorbs while more H_2 is adsorbed onto the Pt surface, thereby decreasing the overall CO conversion. Because the O_2 conversion is approximately 100%, this decrease in CO conversion leads to a decrease in CO selectivity for the metal foam support.

4.3.2 Pt-Fe catalyst (No Pretreatment, Foam/Monolith)

The 400 cpsi ceramic monolith with the 40 ppi, 4% density metal foam were compared. Recall that these two catalysts have the same nominal Pt/Fe washcoat loading of 1.6 g/in^3. Both have a 1" ID and 2" length, with the following conditions: CO = 1.0%, O_2/CO = 1.0, and GHSV = 30,000 hr^{-1}. [The results are summarized in Figure 1 located in the Executive Summary.]

Overall, the CO conversion and selectivity was slightly higher on the metal foam catalyst. At a T_{in}=100°C, the metal foam achieved a 83% CO conversion and a 41% CO selectivity, compared to 79% CO conversion and a 40% CO selectivity on the ceramic monolith. At a higher T_{in}=170°C, the CO conversion and selectivity decreased for both supports, but the metal foam catalyst was still higher for both CO conversion and selectivity – 70% vs. 53%, and 34% vs. 27%, respectively.

Because of the O_2/CO ratio of 1/1 (i.e. twice stoichiometric), the CO selectivity was not high for either temperature. Under all conditions studied, the O_2 conversion reached 90-100%. Since hydrogen oxidation is preferred at higher temperatures, both CO conversion and selectivity decreased when the inlet temperature was increased from 100°C to 170°C.

4.3.3 Pt-Fe catalyst (Pretreatment, Foam/Monolith)

In the case of the 20 ppi, 12% density metal foam, the dramatic drop in CO conversion at T_{in} = 100°C led to an examination of the influence of the pretreatment procedure. The catalysts tested in Figure 5 were not pretreated. Because of the low activity of the 12% density materials, a pretreatment procedure was examined, consisting of two steps: oxidation and reduction. The oxidation consisted of a flow of 10% O_2/balance N_2 gas stream at 230°C for 2 hours to purge and oxidize the catalyst surface. Next, the reduction consisted of a flow of 15% H_2/balance N_2 gas stream, also at 230°C and 2 hours, to reduce the catalyst surface from its' oxidized state. No obvious reactor temperature rise was observed under each pretreatment step.

A retest of the 20 ppi, 12% density metal foam catalyst revealed that after the pretreatment, the CO conversion was much higher than without the pretreatment. At T_{in}=100°C, the CO conversion increased from 15% to 84%. At T_{in}=170°C, the increase was much less, from 62% to 67%. Overall, the CO selectivity was higher for the pretreated catalyst. The effect of the pretreatment on this metal foam is summarized in Figure 6. This increase in activity was permanent; a repeat experiment for the 20 ppi, 12% density foam produced similar results to our first trial.

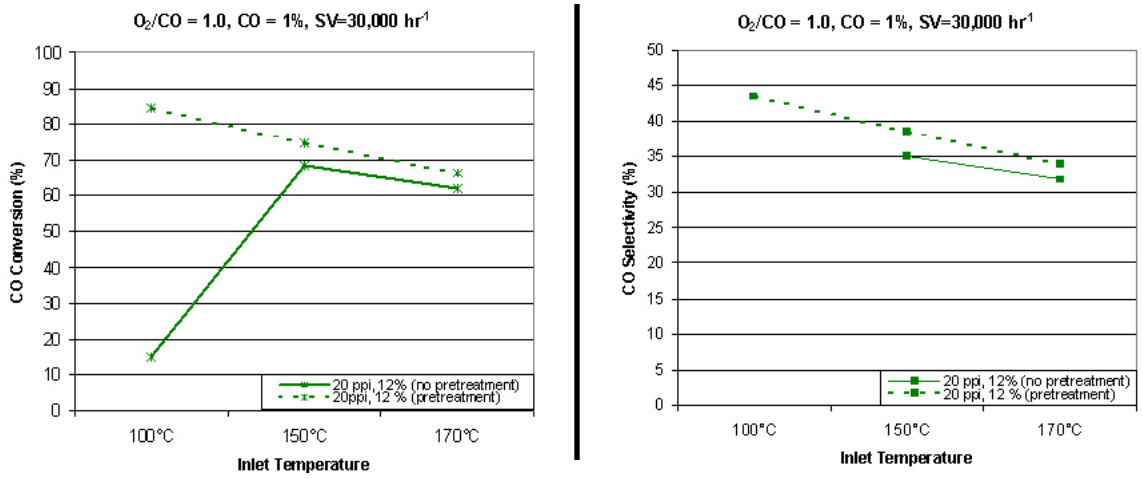

Fig. 6. Effect of Pretreatment on 20 ppi, 12% density metal foam

To see if similar results of pretreatment could be achieved for the catalysts with higher initial activity, the same pretreatment was applied to the 5 wt% Pt-0.5 wt% Fe, 400 cpsi, ceramic straight-channel monolith. There was no significant difference. The ceramic monolith was taken out of the reactor, exposed it to air, and then placed it back in the reactor. This also had no effect. Figures A6 and A7 in Appendix A summarizes these tests.

These data seem to indicate that the use of the pretreatment procedure activated the 20 ppi, 12% density metal foam at low inlet temperatures, but did not effect the catalysts with high activity. Further characterization studies on these supported catalysts are needed to understand the effect of this pretreatment procedure. Information such as washcoat layer thickness, Pt/Fe existing state on the catalyst surface, and Pt/Fe distribution on the metal foam would provide more information to help us understand the effect of pretreatment.

4.3.4 Pt-Fe catalyst (Transients, Foam/Monolith)

To examine any differences between the metal foam and ceramic monolith, a transient study was carried out to test the effect of ΔT_{ad} as a function of time, using a 20 ppi, 12% density metal foam, and a 400 cpsi ceramic monolith. The study was carried out by cutting off the O_2 input, allowing for the outlet temperature to equal the inlet temperature, and then turning the O_2 input back on at time zero. Figure 7 shows the CO and O_2 concentration and outlet temperature from 0 to 15 minutes.

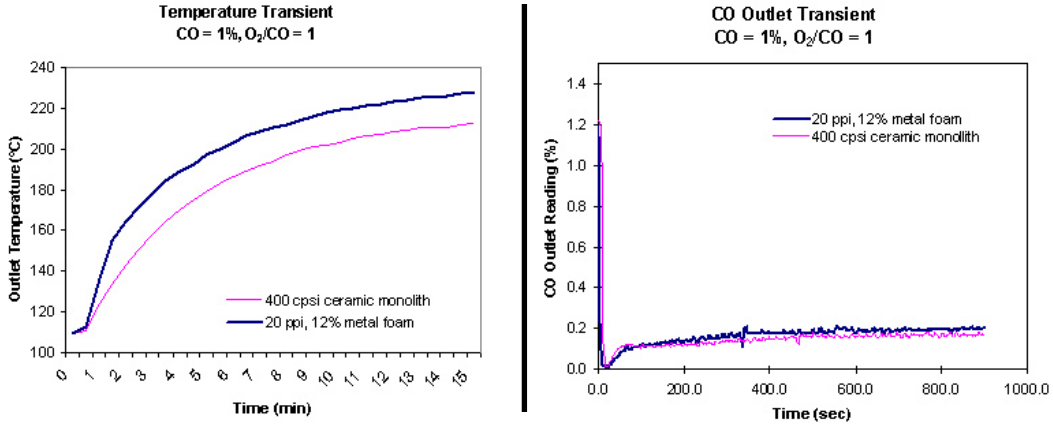

Fig. 7. Temperature and CO Outlet Transient Experiment

The results show that the metal foam responds somewhat more rapidly than the ceramic monolith. This may be caused by the higher thermal conductivity and better radial/axial mixing in metal foams. The CO outlet concentration response is similar for the different supports. More data on the transient behavior can be found in Appendix C.

4.4 Effect of Operating Conditions

4.4.1 O_2/CO Ratio

The effect of the O_2/CO ratio on the CO conversion and selectivity was studied. Figure 8 shows this effect for both the metal foam and ceramic monolith at T_{in}=80°C. For both supports, as the O_2/CO ratio increases, the CO selectivity decreases. This is because more hydrogen is oxidized at higher O_2/CO ratios, especially above stoichiometric values. At higher O_2/CO ratio, the CO conversion increases because of the higher O_2 content in the inlet gas stream.

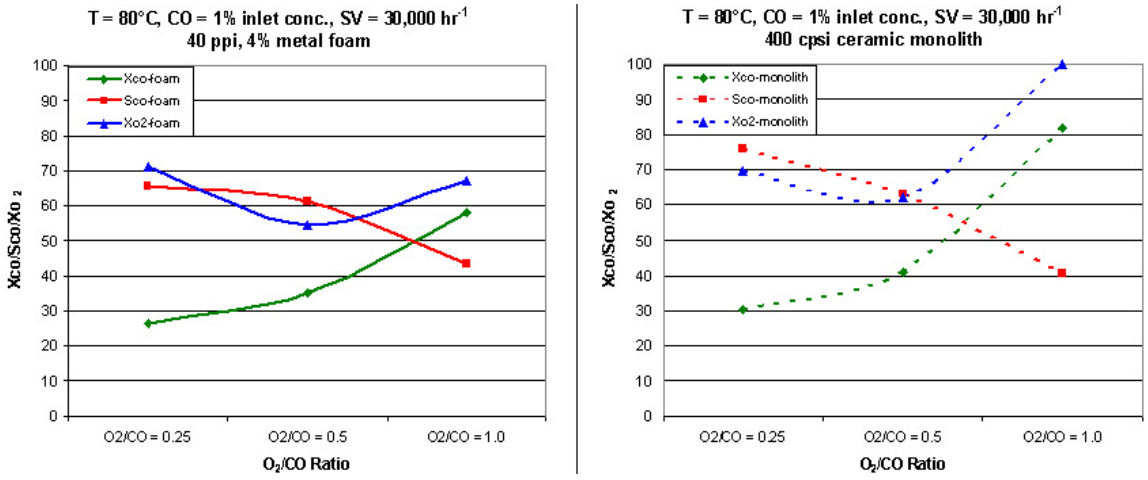

Fig. 8. Effect of O_2/CO ratio on a metal foam and ceramic monolith

Figure A8 in Appendix A shows a performance comparison between the same metal foam and ceramic monolith in Figure 8. In general, the two catalysts were quite

comparable. However, at an O_2/CO ratio = 1.0, the CO conversion for the ceramic monolith was substantially higher than that of the metal foam.

The 40 ppi, 4% density metal foam and the 400 cpsi ceramic monolith used here are not the same piece used in Section 4.3 of this report. We believe that there may be subtle differences between the two different pieces of the same support, despite a conscious effort to synthesize identical catalysts.

4.4.2 Space Velocity / Linear Velocity

A study of GHSV and linear velocity was carried out using 2" and 6" lengths of both the 40 ppi, 4% density metal foam and 400 cpsi ceramic monolith. Figure 9 shows the effect of space velocity on the 40 ppi, 4% density metal foam for a 2" length catalyst piece.

In order to increase the space velocity, the volumetric flowrate through the catalyst was increased; for example, to increase the GHSV from 10,000 hr^{-1} to 30,000 hr^{-1}, the flowrate was increased by a factor of 3, but this also increases the linear velocity by the same factor, shown in equations 13 and 14.

$$\tau = \frac{1}{\text{GHSV}} \tag{12}$$

$$\text{GHSV} = \frac{\dot{V}}{V} \tag{13}$$

$$\dot{V} = \bar{v} A_{xs} \tag{14}$$

τ is defined as the residence (retention) time, GHSV is the gas hourly space velocity, $\dot{V}$ is the volumetric flowrate, V is the catalyst support volume, $\bar{v}$ is the linear velocity, and A_{xs} is the cross-sectional area of the reactor. The linear velocity and space velocity effects are thus coupled in this data, and further tests were carried out in order to decouple the two effects.

The CO and O_2 conversion decreased as the GHSV is increased, while the CO selectivity increased, as expected. CO oxidation is thought to be a faster reaction kinetically than H_2 under certain conditions [**22**]. Therefore, with a shorter retention time, CO selectivity would increase. However, the CO conversion line is flatter than we expected.

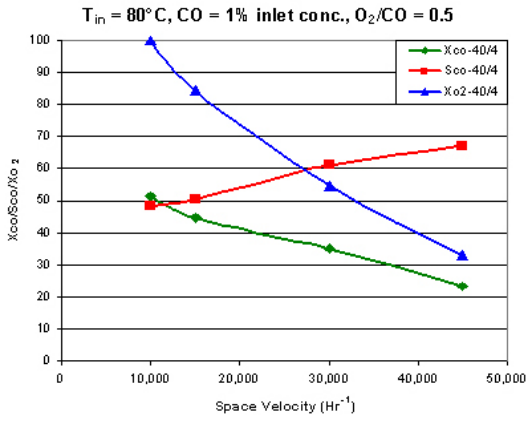

Fig. 9. Effects of GHSV & linear velocity on 40/4 metal foam

To examine this point, CO oxidation is assumed to be a first-order reaction, and the reactor is assumed to be isothermal, which allows the use of a constant value for the reaction rate constant. With these assumptions, the CO conversion at a GHSV of 10,000 hr^{-1} can be calculated to a range of 60%-70%, which is much higher than the measured value of 51%, shown in Figure 9.

Also, the ΔT_{ad} is higher at 10,000 hr^{-1} than at 45,000 hr^{-1} because of the higher O_2 conversion, giving a higher outlet reactor temperature at lower GHSV. Therefore, because of our isothermal assumption, this calculated CO conversion serves as a lower bound on the actual conversion. Calculations are in Appendix D.

One explanation for the "flatness" of the curve of CO conversion as a function of space velocity may be the result of the rWGS reaction, discussed in section 4.2. As the space velocity was reduced, the outlet temperature increased. Therefore, the rWGS reaction may be more important as the GHSV is reduced, potentially accounting for the lowered sensitivity of CO conversion to space velocity.

Another possible explanation is that there are transport effects occurring within our reactor. If the reaction rate is limited by mass transfer of CO or O_2 from the inlet gas stream to the catalyst surface, then the linear velocity through the reactor ($\vec{v}$) would affect the CO conversion. Heat and mass transfer coefficients are positive functions of linear velocity, so as linear/space velocity increases, space velocity reduces the contact time in the reactor, but linear velocity increases the mass transfer coefficient. These competitive effects may cause the behavior of the CO conversion curve as a function of GHSV.

In order to decouple these effects, tests were carried out at fixed space velocity, but varying linear velocities. This was accomplished by placing three 2" 40 ppi, 4% density metal foams together to form a 6" length. The performance of the individual 2" and the 6" metal foam were analyzed. Experimental constraints limited this comparison to GHSV of 10,000 hr^{-1} and 15,000 hr^{-1}. At theses GHSV, the 6" piece had a linear velocity that was three times higher than the 2" piece. The results of this comparison are shown in Figure 10.

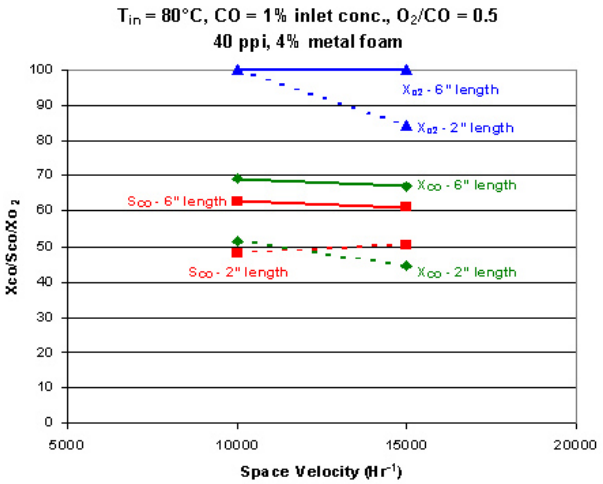

Fig. 10. Effect of linear velocity, constant GHSV

At a constant GHSV, the 6" length reactor piece has an overall higher CO conversion and selectivity, and O_2 conversion, for both GHSV values. This result is consistent with a significant transport resistance between the inlet gas and the surface of the catalyst. The CO and O_2 conversion increases with higher linear velocity because of the increase in the mass transfer coefficient. The CO selectivity is affected because H_2 oxidation is relatively slow compared to the CO oxidation, and therefore not as sensitive to the transport resistance.

Similarly, the linear velocity can be held constant to show the effect of GHSV for the 40/4 metal foam. The linear velocity for a 6" length of catalyst operating at a given space velocity is the same as that for a 2" length of catalyst operating a three times the space velocity. For example, a 6" catalyst running at a GHSV of 5,000 hr^{-1} has the same linear velocity as a 2" catalyst running at a GHSV of 15,000 hr^{-1}. Similarly, the points of 10,000 hr^{-1} and 30,000 hr^{-1}, and 15,000 hr^{-1} and 45,000 hr^{-1}, respectively, have constant linear velocity. [See Equation 13.] Figure 11 shows the results.

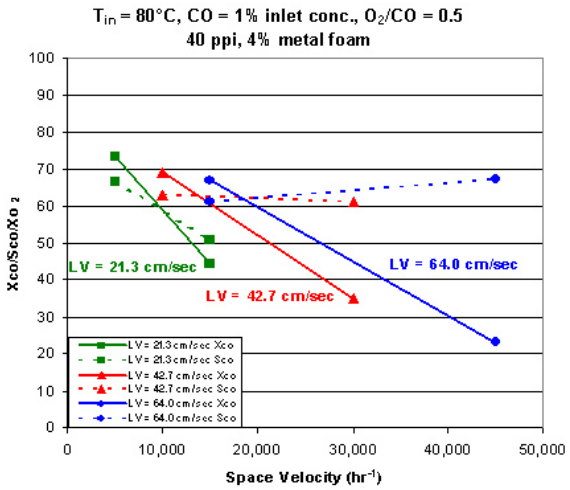

Fig. 11. Effect of GHSV, constant linear velocity

The CO conversion (solid lines), at a constant linear velocity, is much more sensitive to space velocity than seen in Figure 9. From 5,000 hr^{-1} to 15,000 hr^{-1}, at a constant linear velocity of 21.3 cm/sec, the CO conversion drops from 73% to 45%, respectively. Also, note that the CO selectivity (dashed lines) is a function of space velocity. At a linear velocity of 64.0 cm/sec, the CO selectivity increases, but at lower linear velocities (21.3 and 42.7 cm/sec), the CO selectivity decreases or is constant at higher GHSV. At higher space velocities, the CO selectivity should increase because of the shorter retention time and the kinetically faster reaction of CO oxidation, relative to the H_2 oxidation, as explained above.

For the constant linear velocity of 21.3 cm/sec (5,000 hr^{-1} and 15,000 hr^{-1}), the CO conversion would be expected to increase. The O_2 conversion also increases (not shown), from 84% to 100%. However, it seems unlikely that the selectivity for CO oxidation would increase dramatically. Since the reactor is essentially adiabatic, the temperature in the added catalyst segments is higher, and the CO and O_2 concentrations are lower. In general, selectivity would be expected to decrease with increasing temperature and with decreasing CO concentration.

The rWGS reaction offers a possible explanation for this behavior. At lower linear velocities, the catalyst surface can be much hotter than the gas stream temperature. Moreover, the gas stream contains a substantial concentration of H_2, the surface of the catalyst can be higher than the observed ΔT_{ad}. Consequently, the rWGS may be taking place in the first catalyst segment at a higher temperature than that observed leaving the reactor. This will decrease the observed CO conversion and selectivity. However, at lower space velocities, as the gas passes through the second and third section of the 6" catalyst, heat is dissipated as it flows through the different sections, and the temperature difference between the gas stream and the catalyst surface becomes smaller. This allows the rWGS reaction to re-equilibrate at a lower temperature, hence permitting a lower decrease in CO conversion and selectivity.

This effect described above is mitigated at a linear velocity of 64.0 cm/sec. In both the 6" and 2" length reactors, there is much more incomplete combustion (100% and 33% O_2 conversion, respectively), so the ΔT_{ad} is lower for the 2" length, and the catalyst surface may not be significantly hotter than the gas stream. This leads to a higher CO selectivity at faster GHSV, as expected.

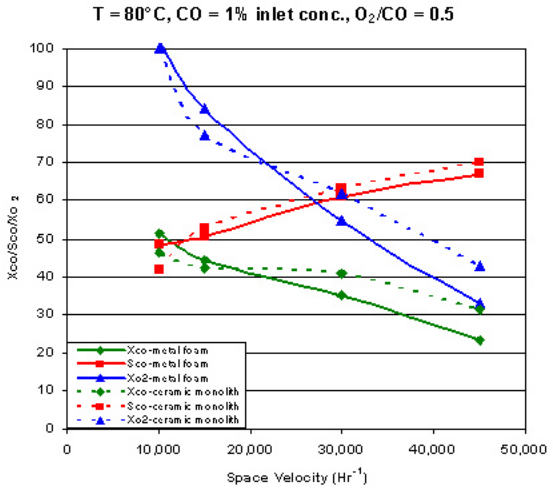

Fig. 12. 40/4 Foam & Monolith comparison

The 400 cpsi ceramic monolith produced similar results to the 40/4 metal foam. Figures A9, A10a, and A10b in Appendix A shows similar results as Figures 9, 10, and 11.

Finally, a comparison of the 40 ppi, 4% density metal foam and the 400 cpsi ceramic monolith reveals that the metal foam is comparable in all aspects to the ceramic monolith. This is depicted in Figure 12.

4.5 Testing of "Identical" Individual Pieces (Ceramic Monolith and Metal Foam)

As noted in section 4.4, the evaluation of the 6" length reactor consisted of three separate, nominally "identical" catalysts for both the metal foam and ceramic monolith reactor. The three pieces are made up of two "new" pieces placed at the beginning and middle of the 6" reactor and one "old" piece placed at the end of the reactor. One of the new pieces was used in section 4.4, while the old piece was used in section 4.3.

The performance of the two "new" pieces of metal foam catalyst was almost identical, but both the CO conversion and selectivity were substantially poorer than those for the original "old" piece. The performance of the two "new" pieces of the ceramic monolith catalyst was not the same. Data is shown in Appendix E.

4.6 Metal Monolith and Ceramic Foam

5% Pt / 0.5% Fe catalysts have also been prepared with the same washcoat loading on a corrugated metal monolith, and a 20 ppi, 11% density ceramic foam. The tests were completed under these conditions: T_{in}= 80°C and 150°C, GHSV=15,000-45,000 hr^{-1}, CO inlet = 1.0%, and O_2/CO ratio = 0.5 and 1.0. The ceramic foam was 1" ID and 2" length, while the metal monolith was 1" ID and 1.5" length. The data is shown in Appendix F.

Under all conditions, the CO and O_2 conversions for the ceramic foam and metal monolith were substantially lower than for the 40/4 "new" metal foam and 400 cpsi "new" ceramic monolith. At T_{in}=80°C, the metal monolith performed higher than the

ceramic monolith in all aspects, but worse than the metal foam and ceramic monolith. At T_{in}=150°C, the metal monolith and ceramic foam had similar CO conversion and selectivity, which were at the same level as the metal foam.

There is no obvious reason why the metal foam and ceramic monolith are distinctly superior. It may be because the preparation techniques for catalysts on ceramic monoliths have been well studied, while the techniques for the newer supports require more study until they are improved.

4.7. ICP/BET (NCSU)

Section 3.2 outlines the procedure used to impregnate the Pt/promoter material and to washcoat the catalyst onto the metal foam. Because metal foams are not of a size that can be fit into characterization systems designed for powder samples, conventional characterization techniques can not be used. Therefore, the powder catalysts prepared were analyzed by two methods. An Inductively Coupled Plasma (ICP)-Emission Spectrometer, at NC State Department of Soil Science, was used to determine bulk elemental composition. Secondly, an in-house Micrometrics Flowsorb II 2300, with Brunauer-Emmett-Teller (BET) capability, was used to determine the total surface area. The results are summarized in Appendix G.

The ICP results show variation between each sample from the projected composition and the determined elemental composition. One sample of specific interest is lab i.d. 80, which is a slurry provided by the Pt-Fe washcoating company. The Fe loading determined is much higher than the projected composition, with a 200% error. This suggests that the samples are not identical.

The BET results show minor variations between each group of samples. The major differences lie within the 5% Pt, varying Fe loadings. This problem is because of inconsistent balance readings.

4.8 BET Surface Area (Clemson)

The BET surface area of the 5 wt% Pt/γ-Al_2O_3 after calcination was 295 m^2/g.

4.9 X-ray Powder Diffusion

The XRD pattern of the Pt catalyst after calcination showed peaks corresponding to γ-Al_2O_3. No peaks for Pt metal were seen. This was due to the high dispersion of the Pt since Cu K_α XRD is not able to detect metal particle sizes less than ca. 5 nm. Overlapping γ-Al_2O_3 peaks also make the detection of Pt peaks even harder.

4.10 Hydrogen Chemisorption

The amount of hydrogen irreversibly chemisorbed on Pt atoms extrapolated to zero pressure was found to be 69.7 μmoles H_2/g cat. The metal dispersion of reduced platinum catalyst was determined to be 54.5%, corresponding to an average Pt particle size of 2.0 nm. This latter quantity was calculated based on the correlation between % dispersion and metal particle size, $\bar{d}_{va} = 6\frac{V_m}{a_m}\Big/ D_m$, where V_m/a_m is the volume per area

of metal atom (V_m=1.46x10^{-23} cm^3/Pt atom, a_m=8x10^{-16} cm^2/ Pt atom) and D_m is the fractional dispersion.

4.11 Catalytic Oxidation of Carbon Monoxide in the Presence of Hydrogen

Time-on-stream (TOS) behavior of CO conversion, rate, and CO_2 selectivity are shown in Figures 2, 3 and 4, respectively, in Appendix B. Both CO conversion and CO_2 selectivity decreased rapidly with TOS. The CO conversion (Figure 2) for the reaction conditions used was 57% at 5-minute TOS and decreased to about 6.5% at reaction steady state. Reaction rate (Figure 3) decreased in a like manner. The results illustrate the rapid deactivation of Pt catalysts typically seen during the initial reaction period. The CO_2 selectivity showed the same decreasing pattern, starting at 90% selectivity and then dropping to 27% within 50 minutes.

Isotopic transient kinetic analysis was used to decouple the deactivation behavior of Pt catalyst into the contributions from site activity and concentration of surface intermediates. Figure 5 in Appendix B gives typical transients for CO, CO_2 and the inert tracer Ar following a step change in the isotopic label on the CO feed. The average surface residence times and concentrations of CO_2 intermediates and reversibly adsorbed CO were calculated using (SS)ITKA software. The switching was conducted at 5 min TOS and periodically afterwards until steady state reaction was reached.

A Langmuir-Hinshelwood single site mechanism is widely accepted to explain CO oxidation on Pt [**2,14,19**]. Adsorbed CO is assumed to react with adsorbed O on an adjacent Pt site. At low reaction temperatures, the noble metal surface is believed to be predominantly covered with adsorbed CO [**14,19**] and the irreversible molecular adsorption of oxygen is suggested to be the rate-determining step. As determined by Nibbelke et al. [**19**], at temperatures between 163-230^{o}C the rate of CO oxidation can be expressed as $R_{CO_2} = const.* P_{O_2} / P_{CO}$.

Although surface reaction is not the rate-determining step, at steady state condition, the rates of all steps including surface reaction are equal and are equivalent to the overall rate of CO oxidation. Therefore the reaction rate can be expressed by

$$R_{CO_2} = const.* P_{O_2} / P_{CO} = \boldsymbol{k_{CO_2} \bullet N_{I-CO_2} \bullet N_O} \qquad (15)$$

where N_{I-CO_2} and N_O are the surface concentrations of CO_2 intermediates and adsorbed oxygen, respectively. Since the surface residence time of CO_2 reaction intermediate $\tau_{CO_2} = N_{I-CO_2} / R_{CO_2}$, the relationship between the intrinsic rate constant k_{CO_2} and τ_{CO_2} is

$$\boldsymbol{1/\tau_{CO_2} = k_{CO_2} \bullet N_O = k = R_{CO_2} / N_{I-CO_2}} \qquad (16)$$

Thus, the reciprocal of the surface residence time of CO_2 intermediate ($1/\tau_{CO_2}$) is equivalent to a pseudo-first-order intrinsic rate constant, *k*, and represents the intrinsic activity of the catalyst (a type of turnover frequency, TOF), although it also includes the oxygen surface concentration dependence, as seen above. However, after varying the

oxygen concentration, it was found that k was weakly dependent on the oxygen concentration.

The dependency of surface concentration and consequent the pseudo-first-order intrinsic rate constant on the partial pressure of oxygen in feed stream is shown in Figure 6 in Appendix B.

Figure 7 in Appendix B shows the TOS behavior of the pseudo-first-order intrinsic rate constant, k. It is obvious that the average intrinsic activity of the Pt sites did not vary greatly with TOS. With the exception of the first data point, k was relatively constant with TOS. The first data point is probably higher due to a higher initial surface concentration of oxygen. On the other hand, as seen in Figure 8 in Appendix B, the concentration of CO_2 surface intermediates decreased with TOS in a similar fashion as the reaction rate (Figure 3, Appendix B). It can be concluded that the deactivation of this Pt catalyst is mainly the result of a decrease in the concentration of active intermediates for CO oxidation (related to the available active Pt sites), not the intrinsic activity.

The concentration of surface Pt atoms calculated from the hydrogen chemisorption measurement was 139 μmoles/g cat. ITKA determined the concentration of surface CO (both reversibly adsorbed, N_{CO} and CO_2 intermediates, N_{I-CO_2}) at 5 min TOS to be 132 μmoles/g cat, about 95% of surface Pt atoms would have been occupied by CO initially. If one assumes that every site was available for reaction at 5 min TOS, this would leave only 7 μmoles/g cat available for the adsorption of hydrogen and oxygen, suggesting the reason for the high selectivity for CO_2 formation. Considering the concentration of surface CO_2 intermediates, N_{I-CO_2}, it would appear that the surface coverage in intermediates, calculated by dividing N_{I-CO_2} with the concentration of surface Pt atoms, was only 41% at 5 minute TOS. At steady state, the concentration of active CO_2 intermediates decreased to about 7% coverage. This decrease is reflected in the decrease in CO oxidation rate and CO_2 selectivity. Although the surface coverage of CO_2 intermediates decreased about 80%, the surface coverage of reversibly adsorbed CO increased only 30%. Although the CO oxidation rate decreased, the H_2 oxidation rate increased from ca. 0.92 μmoles/g cat/s at 5 min TOS to ca. 2.4 μmoles/g cat/s at steady state. This might suggest that hydrogen has better able to compete for oxygen because of the decrease in concentration of CO_2 intermediates. The decrease in CO_2 selectivity is, thus, the result of the decrease in CO oxidation rate and the concomitant increase in H_2 oxidation rate. By assuming that all Pt surface atoms are active for CO oxidation, the TOF based on hydrogen chemisorption calculated (~0.007 sec^{-1}) was about 12 times lower than the pseudo-first-order steady state rate constant (~0.09 sec^{-1}) at steady state condition.

4.12 Characteristics of the catalyst surface at steady state

In order to determine the cause of deactivation, additional experiments were conducted to try to determine the surface composition of the catalyst after reaction.

4.12.1 Effect of regeneration temperature

The deactivated catalyst was regenerated at different temperatures in a stream of hydrogen for 1 h. As shown in Figure 9 in Appendix B, some of initial activity was recovered using regeneration temperatures lower than 300^{o}C. On the other hand, regeneration at temperatures higher than or equal to 300^{o}C resulted in a complete recovery of the initial activity.

4.12.2 Effect of CO addition before oxygen

The catalyst bed was flushed with the reactant stream excluding oxygen for 1 h before adding oxygen and starting the CO oxidation reaction. At 5 minute TOS (after oxygen was fed), the CO oxidation rate was found to be approximately the same as the rate at steady state (after deactivation) in the normal run. This result suggests that CO is the source of the species that deactivates the catalyst.

4.12.3 Hydrogen reaction with the deactivated catalyst

About 50% hydrogen in helium was fed through the bed of partially deactivated catalyst after reaching steady state while the temperature in the reactor was raised from the reaction temperature to 550^{o}C. A mass spectrometer was used to detect the gas outlet composition from the reactor. Small amounts of methane were detected in the temperature range of 230^{o}C to 280^{o}C.

4.12.4 Determination of carbon content

After reaching steady state reaction rate, a sample of the deactivated catalyst was removed and sent to Galbraith, Inc. for carbon determination. The amount of carbon determined by from the combustion/coulometric titration was 16.7 μmole/g cat, equivalent to 12% coverage of the surface Pt atoms by carbon atoms.

5. Conclusions

A series of Fe-promoted Pt/Al_2O_3 catalysts were synthesized and evaluated for the selective oxidation of a low concentration of CO in the presence of a high concentration of H_2. Very strong inhibition by CO was observed for catalyst with a 0.5 wt% Pt / 0.005 wt% Fe / Al_2O_3 washcoat, with a 1.6 g/in^3 loading on the support. The CO in the inlet gas stream poisons the catalyst, but the inhibition is reversible, as seen when CO is removed from the inlet gas stream.

A ceramic monolith support with a washcoat loading containing 5 wt% Pt and 0.5 wt% Fe proved to have a high activity for CO conversion, along with a moderate selectivity for CO over H_2. With an inlet temperature of 100^{o}C, and 1.0% CO and an O_2/CO ratio = 1.0 in the feed gas, this catalyst was able to achieve 80% conversion with a selectivity of about 40%. Because the tests were carried out above stoichiometric O_2 concentrations, the CO selectivity can only reach a maximum of 50% if all the O_2 is oxidized.

Different metallic foams were tested as catalyst supports. In general, the best foam structure was the 40 ppi, 4% density. Catalysts prepared on this foam had comparable activity and selectivity to the 400 cpsi ceramic, straight-channel monolith. Catalysts prepared on the 40/4 foam gave a slightly higher performance than the 20/4 foam, and significantly higher than the 40/12 and 20/12 catalysts. However, the apparent differences between these four supports, and the individual "identical" pieces of the 6" reactor study, may reflect the inconsistencies of reproducible catalyst preparation on a novel support. Further attention is required on the techniques for both catalyst preparation and catalyst characterization. To increase the CO conversion, a pretreatment method increased the activity of low performance catalysts, but did not impact already high performance catalysts.

Studies on catalyst prepared with the 5 wt% Pt/0.5 wt% Fe washcoat showed that the reverse water-gas-shift reaction played an important role in determining CO conversion and selectivity, especially at higher inlet temperatures. This reaction needs to be suppressed in order for us to reach feasible CO concentrations.

Metal monoliths and 20/11 density ceramic foams were also evaluated, but had lower activity and selectivity. Further work was done on transient behaviors in order to discover differences between the metal foam and ceramic monolith support, but no significant difference was determined.

Various operating conditions were examined, specifically: O_2/CO ratio, space velocity, and linear velocity. Studies showed that the performance of the catalysts prepared on both the ceramic monolith and the metal foam was influenced by mass and heat transport, to some extent. The transport characteristics of straight-channel monoliths are reasonably well understood. However, additional work to quantify the mass- and heat-transfer characteristics of the metal foams is necessary.

The selective oxidation of CO in the presence of hydrogen using 5% Pt/γ-Al_2O_3 exhibited high initial partial deactivation before reaching steady state. The observed rate and CO_2

selectivity were very high during the initial reaction period, but decreased significantly with time-on-stream. By using isotopic transient analysis, the pseudo-first-order intrinsic rate constant was found to be relatively constant compared to the concentration of surface CO_2 reaction intermediates. It can be concluded that the deactivation of this Pt catalyst is mainly the result of a decrease in the concentration of surface intermediates, not the intrinsic activity. In addition, regeneration of the catalyst in the stream of hydrogen at temperatures higher than or equal to 300^{o}C can completely recover the initial activity and selectivity of the deactivated catalyst. Approximately 12% of surface Pt was likely covered with carbonaceous species during initial deactivation. From this result, we suggest that the deactivation of Pt is due to carbon deposition on the Pt surface and that this carbon deposition also caused a significant decrease in CO_2 selectivity. Possibly CO_2 selectivity is decreased because CO adsorption is affected more than H_2 and O_2 adsorption.

6. Recommendations

a) Develop reproducible techniques for catalyst preparation. The Pt/Fe system that was investigated appears to have promise and is worthy of further study, but the results on nominally identical foams were somewhat different. Re-evaluate other foam structures once reproducible catalyst preparation techniques have been established.

b) In connection with catalyst preparation research, develop techniques to characterize these catalysts, including measuring washcoat uniformity, Pt metal area, and Fe dispersion, and other surface properties. Typical characterization techniques are not feasible with these support systems because of their shapes and sizes. Novel methods will be needed to characterize the foams used in these tests.

c) Carry out additional research to define the transport effects on metal foams and ceramic straight-channel monoliths. This includes measuring the mass transfer characteristics of the foams.

d) Evaluate the need for an isothermal reactor. The adiabatic temperature rise plays a significant role in the rWGS reaction. To suppress this reaction, catalysts on metal foams with cooling tubes inserted metallurgically should be reviewed.

e) Evaluate the reactions in the kinetic regime to determine kinetic rate constants and develop a model. This involves the use of a differential reactor.

f) Assess the use of other metal promoters from the Straschil and Egbert patent [**3**], such as Mn, Co, Sn.

7. References

1. Korotkikh, O. and R. Farrauto, *Catalysis Today*, 62 (2002), 249-254.

2. Liu, X., O. Korotkikh and R. Farrauto, *Applied Catalysis A*, 226 (2002), 293-303.

3. Straschil, H.K. and W. Egbert, Canadian Patent CA 828058, Nov. 25, 1969.

4. Oh, S.H. and R.M. Sinkevitch, *Journal of Catalysis*, 142 (1993), 257-262.

5. Venderbosch, R.H., W. Prins, P.M. van Swaaij, *Chemical Engineering Science*, 53 (1998), 3355-3366.

6. Farrauto, R.J. and C.H. Bartholomew, Fundamentals of Industrial Catalytic Processes, Blackie Academic (New York), (1997) 38-39, 358.

7. Anderson, J.R. and K.C. Pratt, Introduction of Characterization and Testing of Catalysts, Academic Press Inc. (London) (1985), 3-6.

8. DeWild, P.J., M.J. Veehaak, D.F. Bakker, PCT Appl. WO 00/17097, Mar. 30, 2000.

9. Manasilp, A. and E. Gulari, *Applied Catalysis B*, 37 (2002), 17-25.

10. Grigorova, B., J. Mellow, A. Palazov, F. Greyling, PCT Appl. WO 00/59631, Oct. 12, 2000.

11. Rohland, B. and V. Plzak, *Journal of Power Sources*, 84 (1993), 183-186.

12. Gotz, M. and H. Wendt, *Electrochimica Acta*, 43 (1998), 3637-3644.

13. Igarashi, H., H. Uchida, M. Suzuki, Y. Sasaki, M. Watanabe, *Applied Catalysis A*, 159 (1997), 159-169.

14. Kahlich, M. J., Gasteiger, H. A., and Behm, R. J., *Journal of Catalysis* **171**, 93 (1997).

15. Grunwaldt, J.-D., Maciejewski, M., Becker, O. S., Fabrizioli, P., and Baiker, A., *Journal of Catalysis* **186**, 458 (1999)

16. Kahlich, M.J., Gasteiger, H. A., and Behm, R. J., *Journal of Catalysis* **182**, 430 (1999).

17. Bethke, G. K., and Kung, H. H., *Applied Catalysis A* **194,** 43 (2000).

18. Grisel, R. J. H., and Nieuwenhuys, B. E., *Journal of Catalysis* **199**, 48 (2001).

19. Nibbelke, R. H., Campman, M. A. J., Hoebink, J. H. B. J., and Marin, G. B., *Journal of Catalysis* **171**, 358 (1997).

20. Shannon, S. L., and Goodwin, J. G., Jr., *Chemical Review* **95**, 677 (1995).

21. Hammache, S., Shannon, S. L., Kim, S. Y., and Goodwin, J. G., Jr. in "Encyclopedia of Surface & Colloid Science"; Ed. A. Hubbard, Marcel Dekker Inc., p.2445-2454 (2002).

22. Kim, D.H. and M.S. Lim, *Applied Catalysis A*, 224 (2002), 27-38.

8. Bibliography

9. List of Acronyms and Abbreviations

40/4	40 ppi, 4% density foam
20/4	20 ppi, 4% density foam
40/12	40 ppi, 12% density foam
20/12	20 ppi, 12% density foam
ΔH_{rxn}	Heat of Reaction
ΔT_{ad}	Adiabatic Temperature Rise
BET	Brunauer-Emmett-Teller
C_p	Heat Capacity
cpsi	Cells Per Square Inch
GHSV	Gas Hourly Space Velocity
ICP	Inductively Coupled Plasma
ITKA	Isotopic-Transient Kinetic Analysis
I.D.	Inner Diameter
LV	Linear Velocity
NDIR	Nondispersive Infrared
PEM	Proton Exchange Membrane
ppi	Pores Per Inch
PROX	Preferential Oxidation
rWGS	Reverse Water-Gas-Shift
S_{CO}	CO selectivity
SSITKA	Steady-State Isotopic-Transient Kinetic Analysis
T_{in}	Inlet Gas Stream Temperature
TCD	Thermal Conductivity Detector
TOF	Turnover Frequency
TOS	Time-On-Stream
UHP	Ultra-High Pure
X_{CO}	CO conversion
X_{O2}	O_2 conversion
XRD	X-Ray Powder Diffusion

Appendix A

NCSU Figures

(a)

(b)

(c)

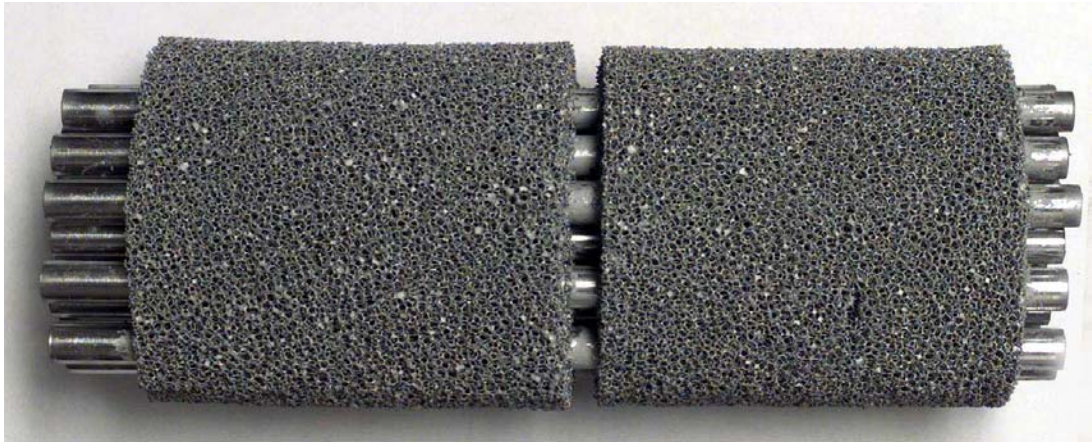

Fig. A1. Pictures of (a) open cells in metal foam, (b) shapes of metal foams, and (c) metal tubes inserted into metal foams

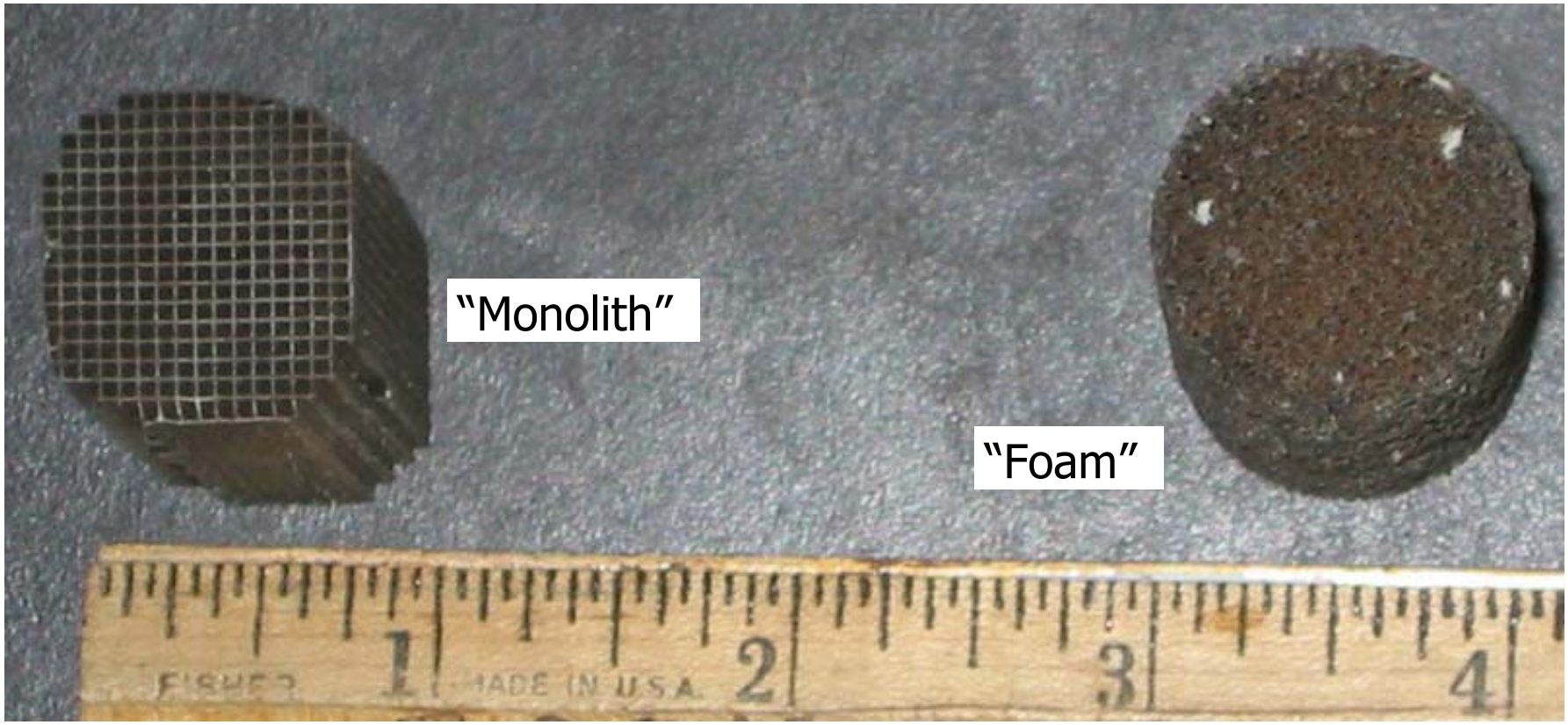

Fig. A2. 400 cpsi Ceramic Straight-Channel Monolith ("monolith") and a 40 ppi, 4% density Metal Foam ("foam")

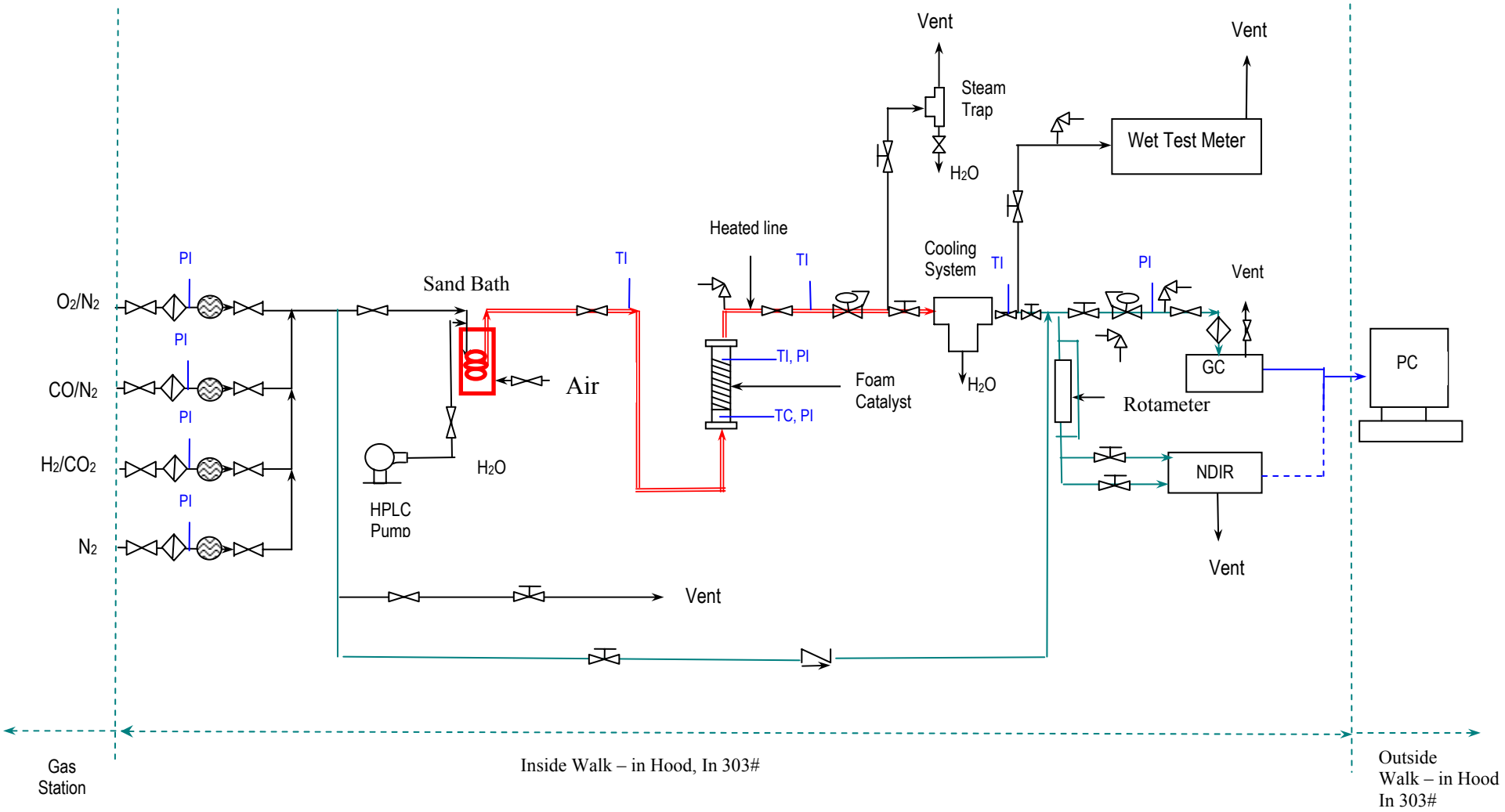

Fig. A3. Process Flowsheet for our PROX System

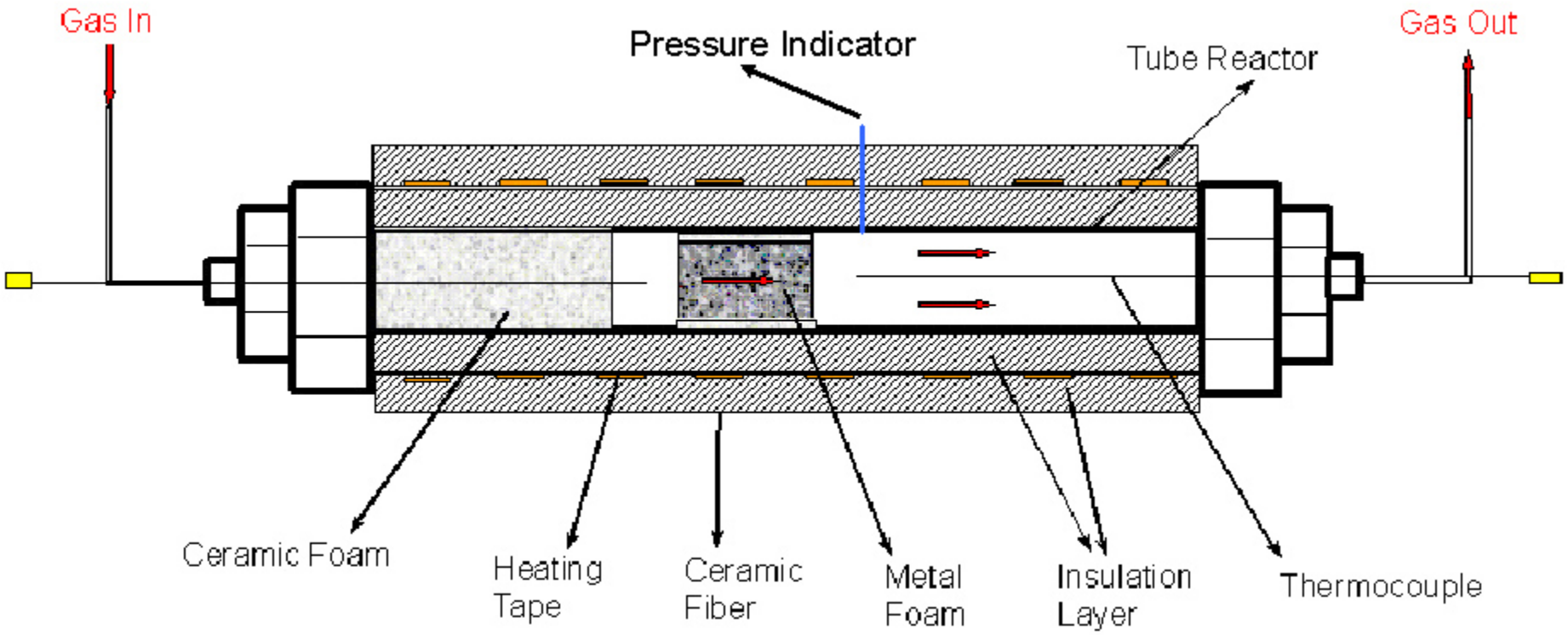

Fig. A4. Reactor Design Schematic

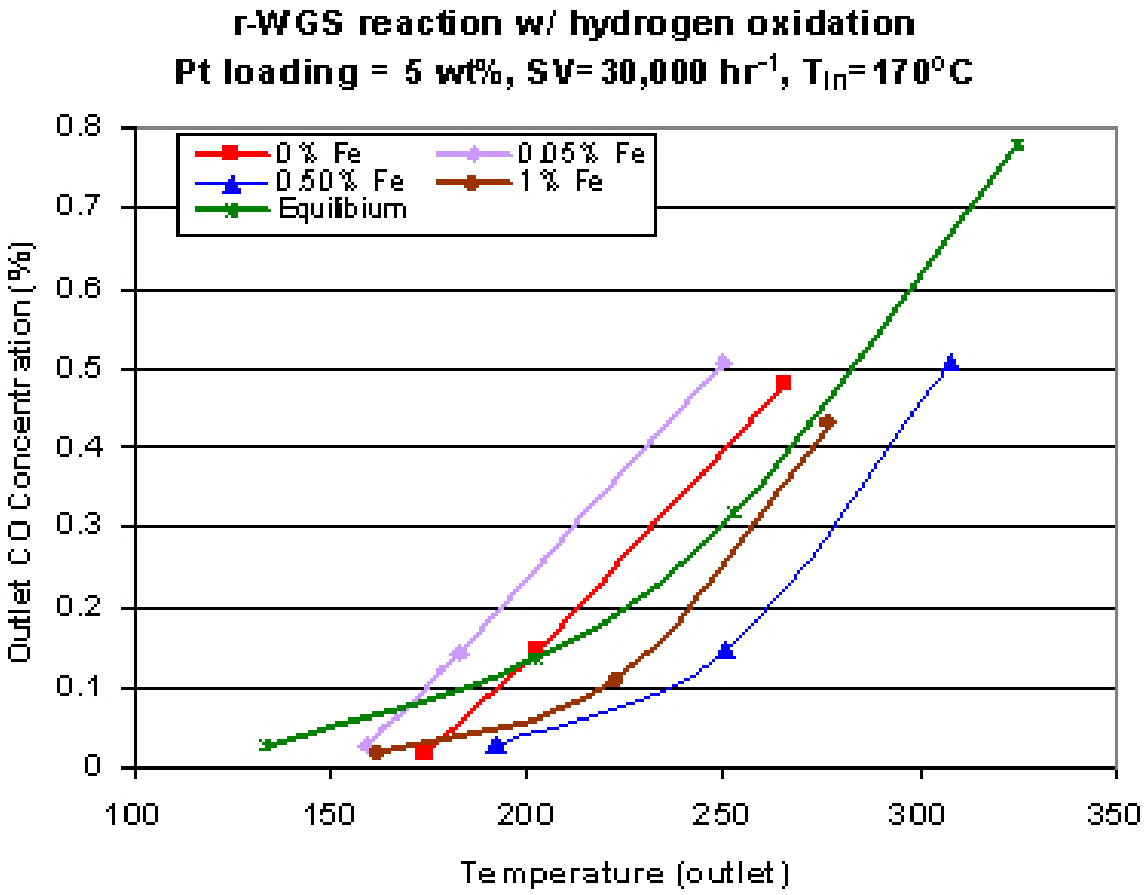

Fig. A5. Effect of rWGS on 400 cpsi ceramic monolith, varying Fe wt% loading

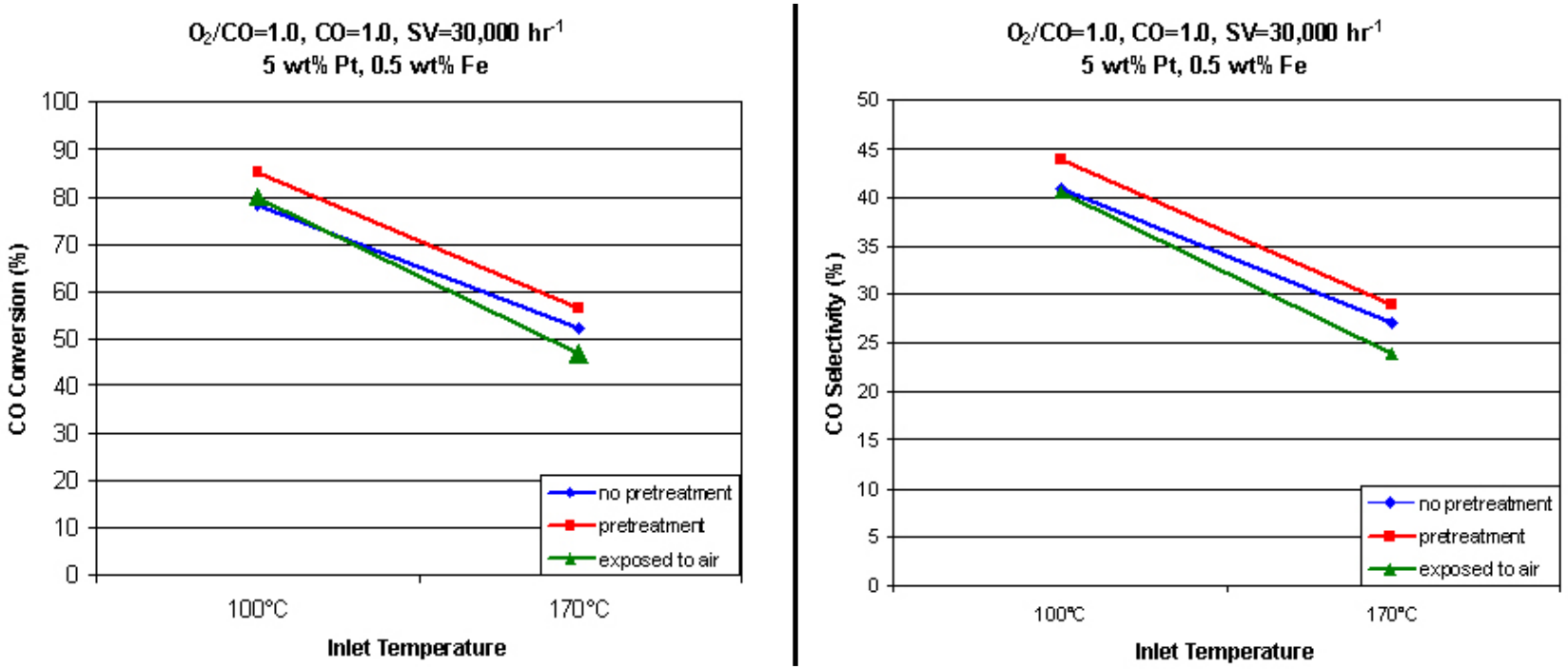

Fig. A6. Effect of Pretreatment on 400 cpsi Straight-Channel Ceramic Monolith

Fig. A7. Effect of Pretreatment for Monolith and Foam, Tabular Form

THE EFFECT OF PRETREATMENT (based on CO conversion)

20 ppi, 12% density metal foam support

		No pretreatment	After Pretreatment	Pretreatment + Rexposure to Air
100°C	$CO/O_2 = 1$	14.70%	83.70%	80.40%
	$CO/O_2 = 0.5$	9.00%	55.30%	55.40%
170°C	$CO/O_2 = 1$	61.90%	67.00%	48.10%
	$CO/O_2 = 0.5$	47.20%	54.50%	46.80%

400 cpsi ceramic monolith

		No pretreatmen	After Pretreatmen	After Pretreatment (Re.)
100°C	$CO/O_2 = 1$	78.80%	85.40%	88.00%
	$CO/O_2 = 0.5$	59.60%	52.10%	59.40%
170°C	$CO/O_2 = 1$	53.10%	57.40%	
	$CO/O_2 = 0.5$	58.60%	49.00%	

Main Conclusions:

1. Pretreatment improved 20 ppi, 12% density metal foam catalyst performance.
This improvement also seems to be permanent since the CO conversion was considerably same before and after air exposure for the pretreated sample.

2. Pretreatment slightly improved ceramic monolith performance with some conditions ($O_2/CO = 1$).
With $O_2/CO = 0.5$ condition, CO conversion was even marginally lower than before (without pretreatment). Overall, pretreatment did not have an impressive effect on the performance of ceramic monolith.

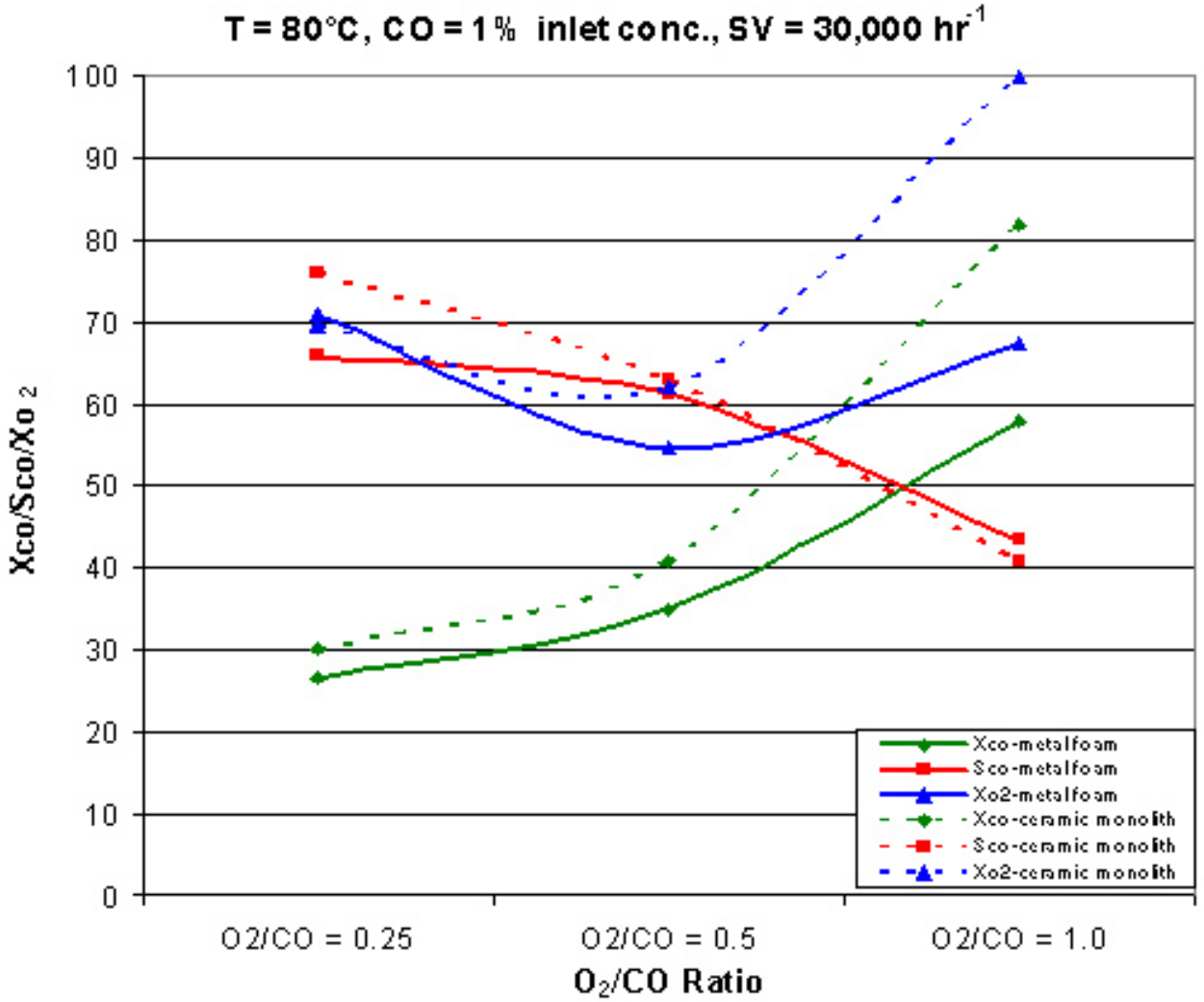

Fig. A8. Comparison of Effect of O_2/CO on 40/4 metal foam and 400 cpsi ceramic monolith

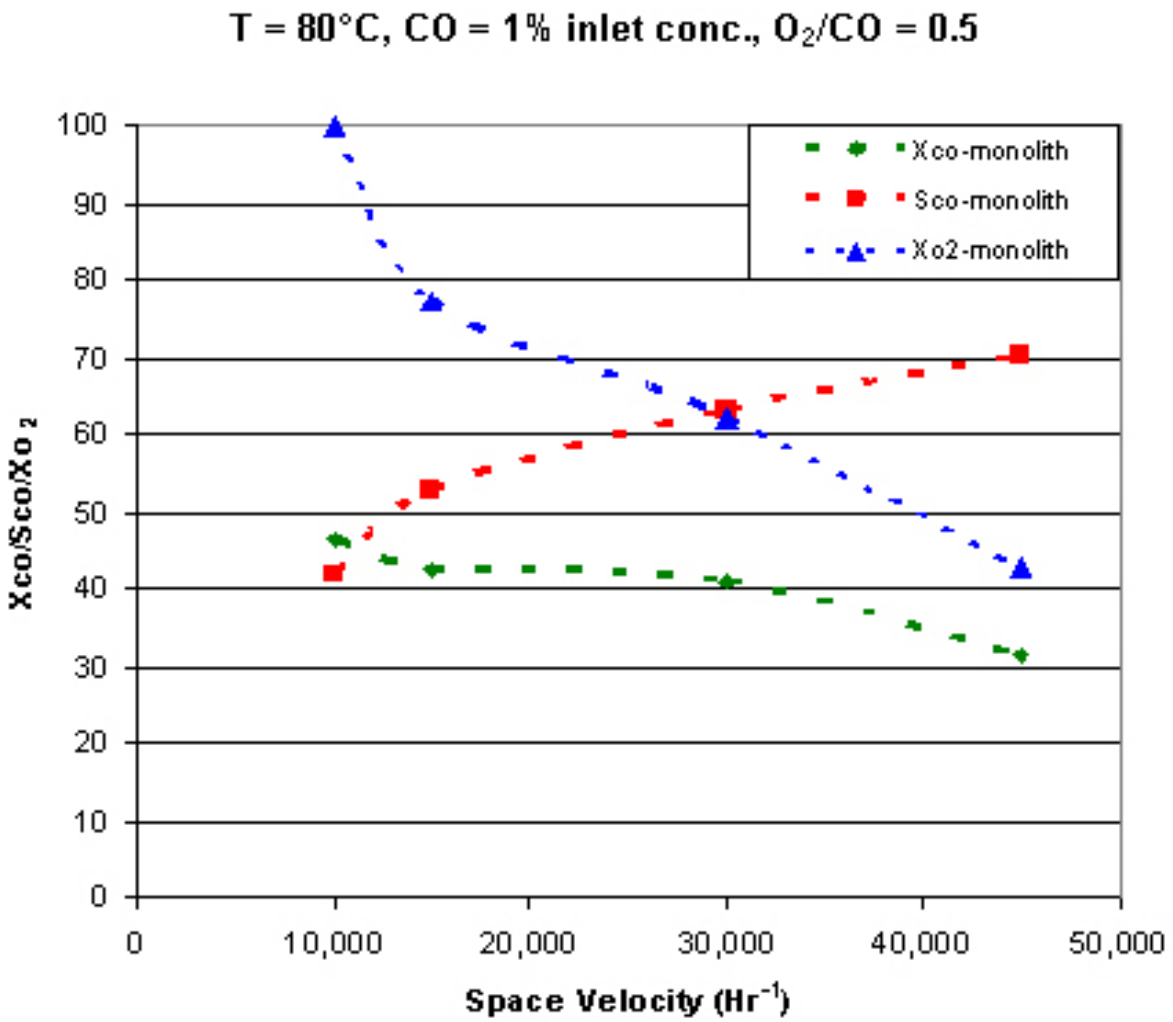

Fig. A9. Effects of GHSV and linear velocity on 400 cpsi ceramic monolith

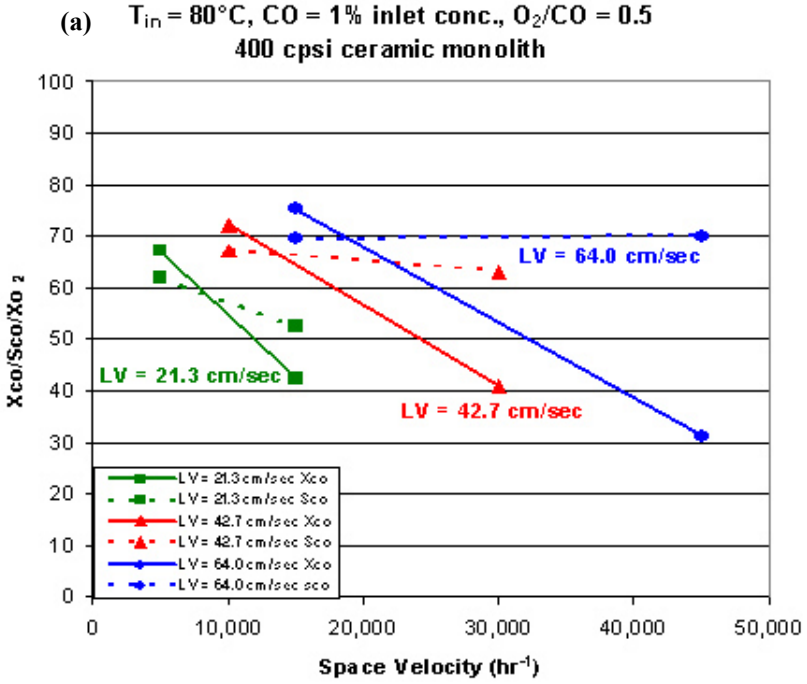

Fig. A10a. Effect of GHSV, constant linear velocity

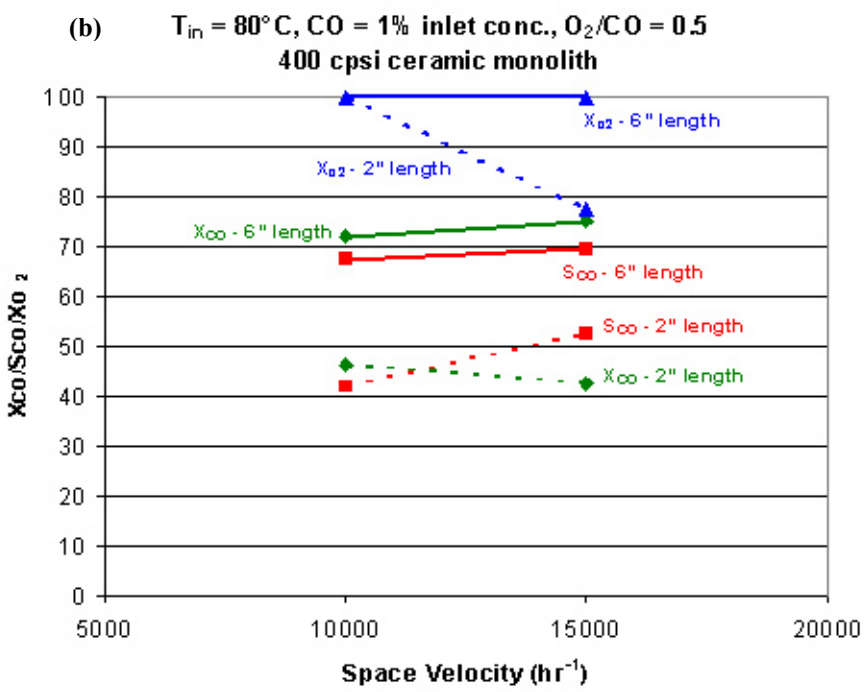

Fig. A10b. Effect of linear velocity, constant GHSV

Appendix B

Clemson Figures

Table 1. Isotopic transient kinetic analysis results

TOS (min)	**CO Conversion** (%)	**Rate**[a] (μmole/g cat/sec)	τ_{CO_2} (sec)	τ_{CO} (sec)	N_{I-CO_2} (μmol/gcat)	N_{CO} (μmol/g cat)	k[b] (sec^{-1})	$N_{(I-CO_2+CO)}$ (μmol/g cat)	θ_{I-CO_2}[c]	θ_{CO}[c]	$\theta_{(I-CO_2+CO)}$[c]
5	57.68	8.30	6.9	4.0	57	75	0.145	132	0.41	0.54	0.95
10	21.43	3.08	11.3	5.0	35	72	0.088	106	0.25	0.51	0.76
15	11.44	1.65	9.5	5.4	16	78	0.105	93	0.11	0.56	0.67
20	11.52	1.66	10.7	6.2	18	89	0.094	107	0.13	0.64	0.76
30	7.95	1.14	9.9	6.1	11	87	0.101	99	0.08	0.63	0.71
35	7.90	1.13	11.6	6.8	13	98	0.086	111	0.10	0.70	0.80
40	6.46	0.93	10.4	6.6	10	96	0.096	105	0.07	0.68	0.75
55	6.53	0.94	10.8	6.1	11	88	0.092	99	0.08	0.63	0.71
160	6.19	0.89	11.5	6.7	10	97	0.087	107	0.07	0.70	0.77

[a] Rate = micromoles of CO consumed per gram of catalyst per second at 90°C; 1.8 atm; 45% H_2, 1% O_2, 1% CO by mole and balance He

[b] $k=1/\tau_{CO_2}$, pseudo-first-order intrinsic rate constant. Error estimated at ±5%

[c] $\theta_i = N_i$/(irreversibly adsorbed H atom), the surface coverage of species i. Error estimated at ± 10%

Figure Captions

Figure 1: Schematic diagram of the ITKA CO oxidation system.

Figure 2: Time-on-stream behavior for CO conversion at 90^{o}C.

Figure 3: Time-on-stream behavior for the CO oxidation rate at 90^{o}C.

Figure 4: Time-on-stream behavior for CO_2 selectivity during CO oxidation at 90^{o}C.

Figure 5: Isotopic transients during CO oxidation at 90^{o}C on 5% Pt/γ-Al_2O_3 at steady state.

Figure 6. Oxygen partial pressure dependency of surface oxygen concentration

Figure 7: Time-on-stream behavior of the pseudo-first-order intrinsic rate constant at 90^{o}C.

Figure 8: Time-on-stream behavior of the concentration of CO_2 surface intermediates, N_{I-CO_2}, at 90^{o}C.

Figure 9: Time-on-stream behavior of the CO oxidation rate after regeneration at different temperatures.

.

Fig. 1

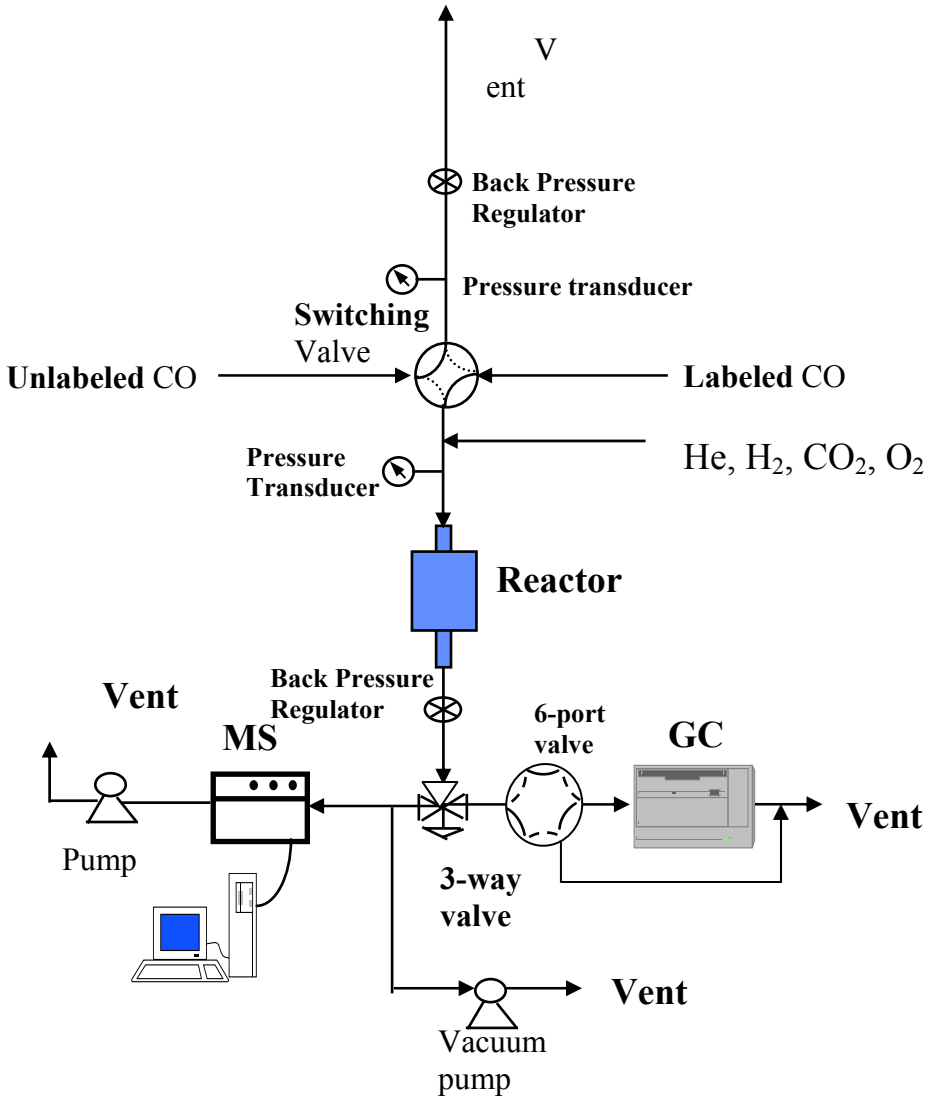
V
ent
Back Pressure
Regulator
Pressure transducer
Switching
Valve
Unlabeled CO
Labeled CO
Pressure
Transducer
He, H2, CO2, O2
Reactor
Vent
Back Pressure
Regulator
MS
6-port
valve
GC
Vent
Pump
3-way
valve
Vent
Vacuum
pump

Fig. 2

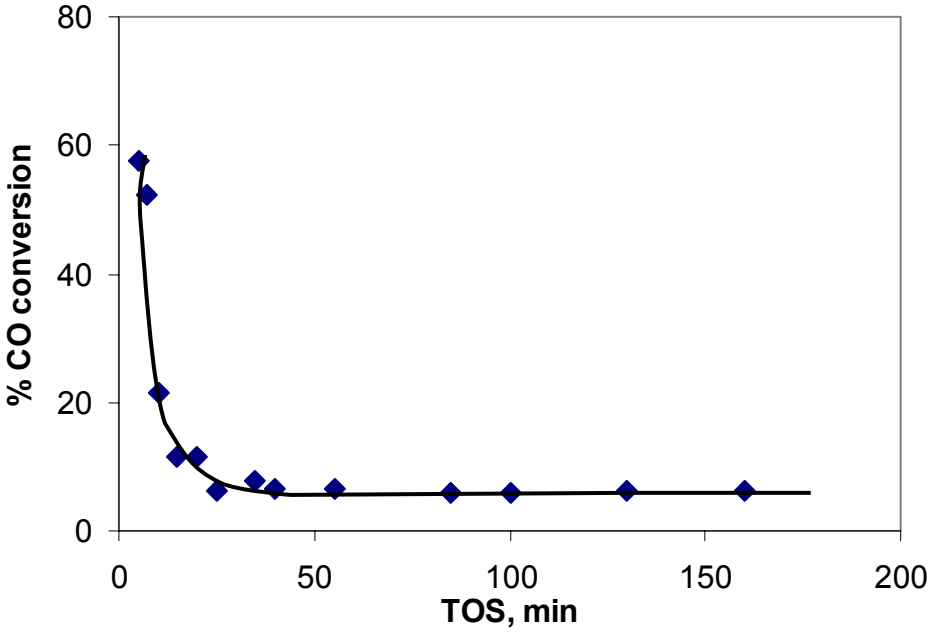

Fig. 3

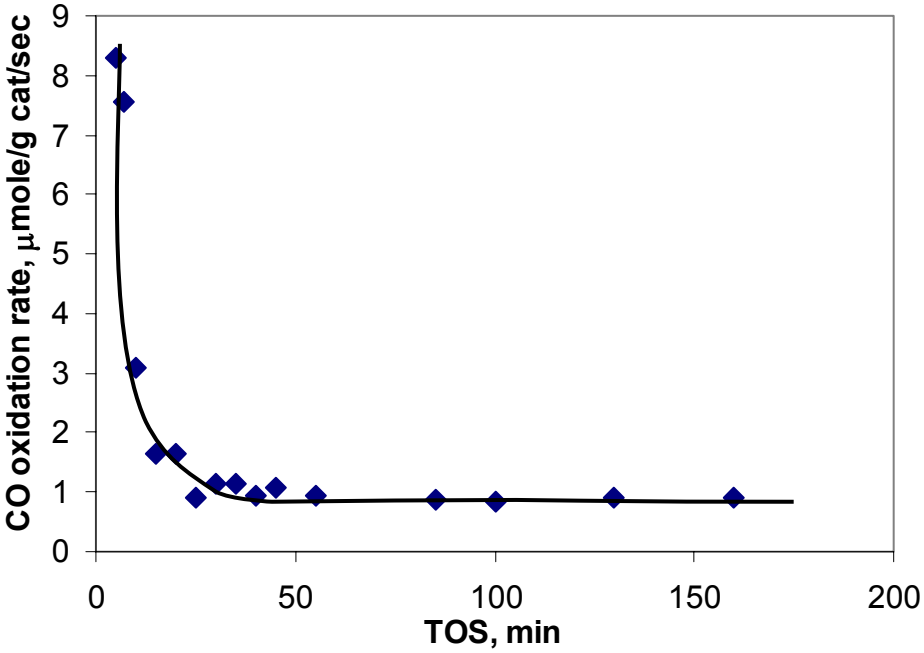
CO oxidation rate, μmole/g cat/sec
0
1
2
3
4
5
6
7
8
9
0
50
100
150
200
TOS, min

Fig. 4

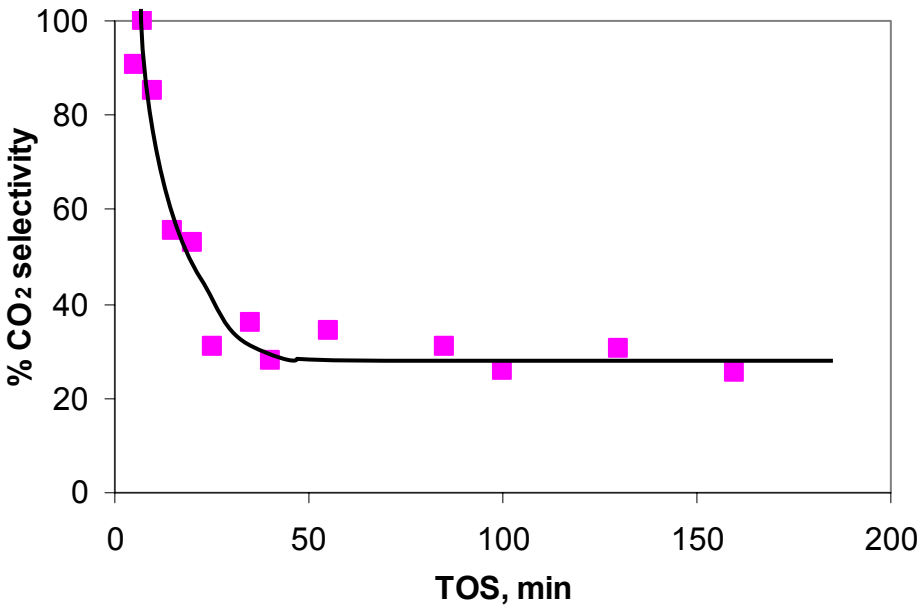

Fig. 5

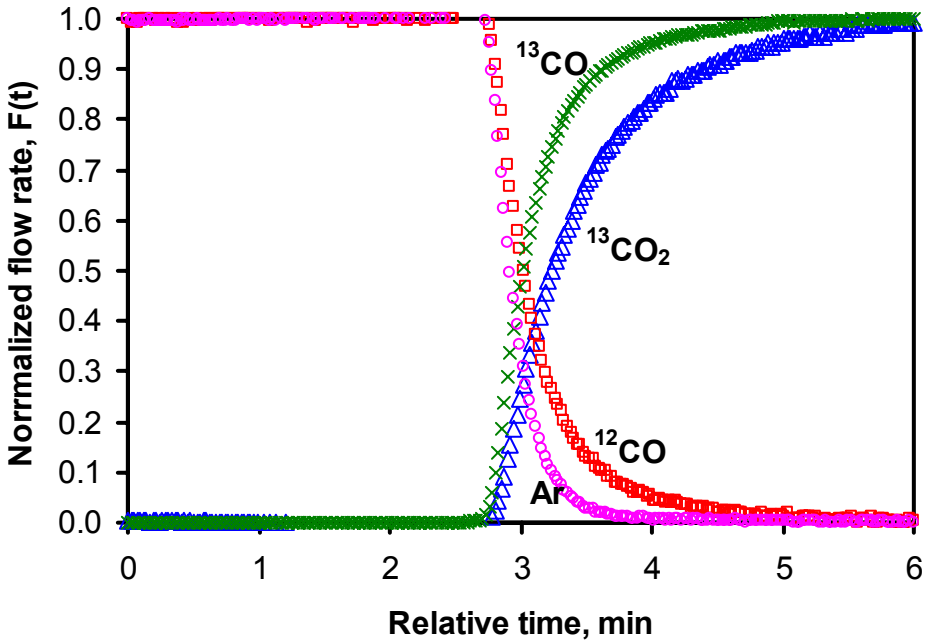
Normalized flow rate, F(t)
1.0
0.9
0.8
0.7
0.6
0.5
0.4
0.3
0.2
0.1
0.0
0
1
2
3
4
5
6
Relative time, min
13CO
13CO2
12CO
Ar

Fig. 6

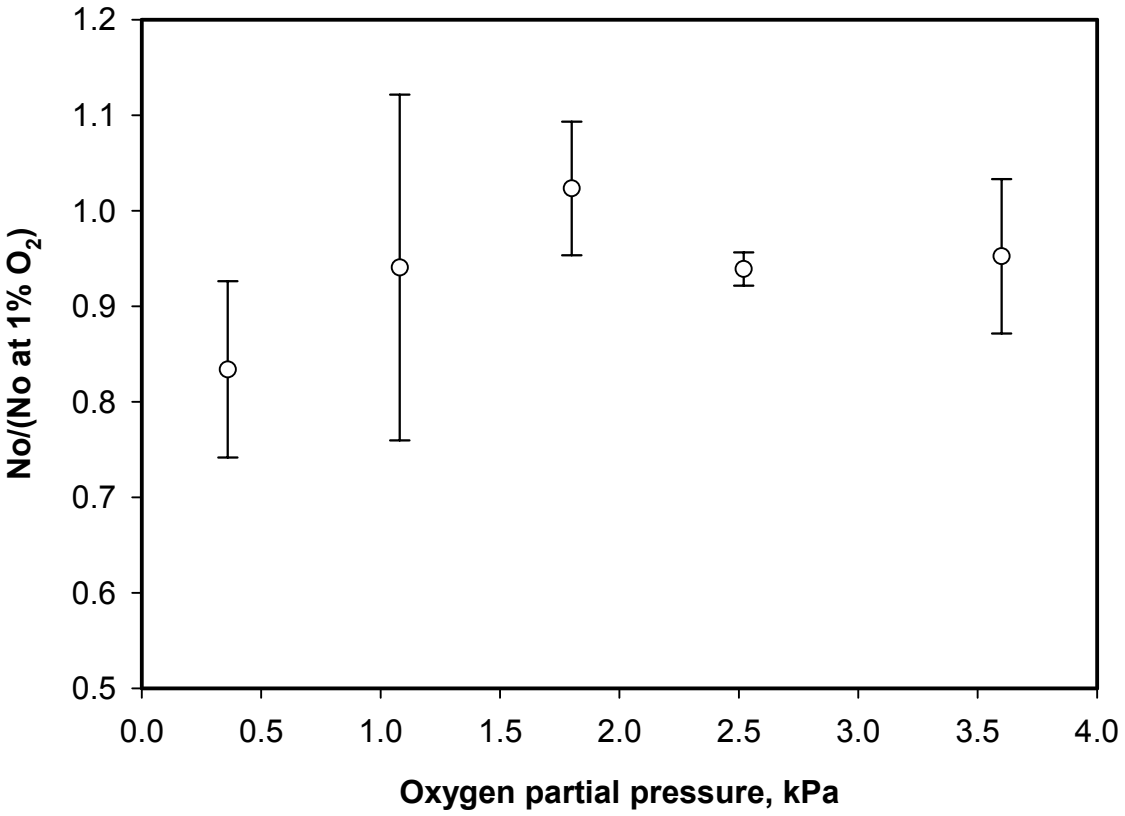
1.2
1.1
1.0
0.9
0.8
0.7
0.6
0.5
No/(No at 1% O2)
0.0
0.5
1.0
1.5
2.0
2.5
3.0
3.5
4.0
Oxygen partial pressure, kPa

Fig. 7

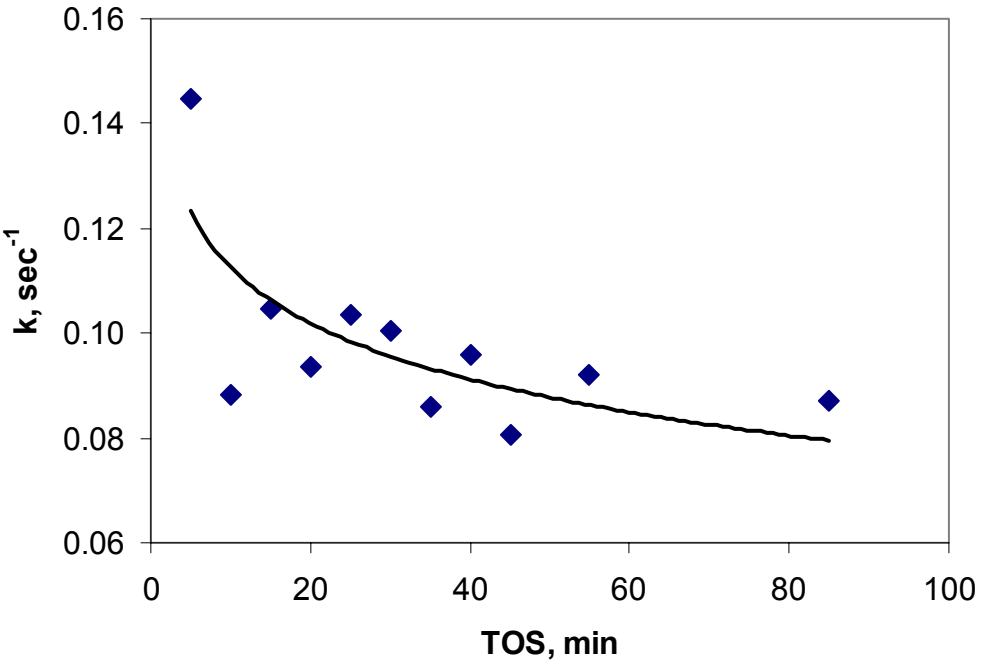

Fig. 8

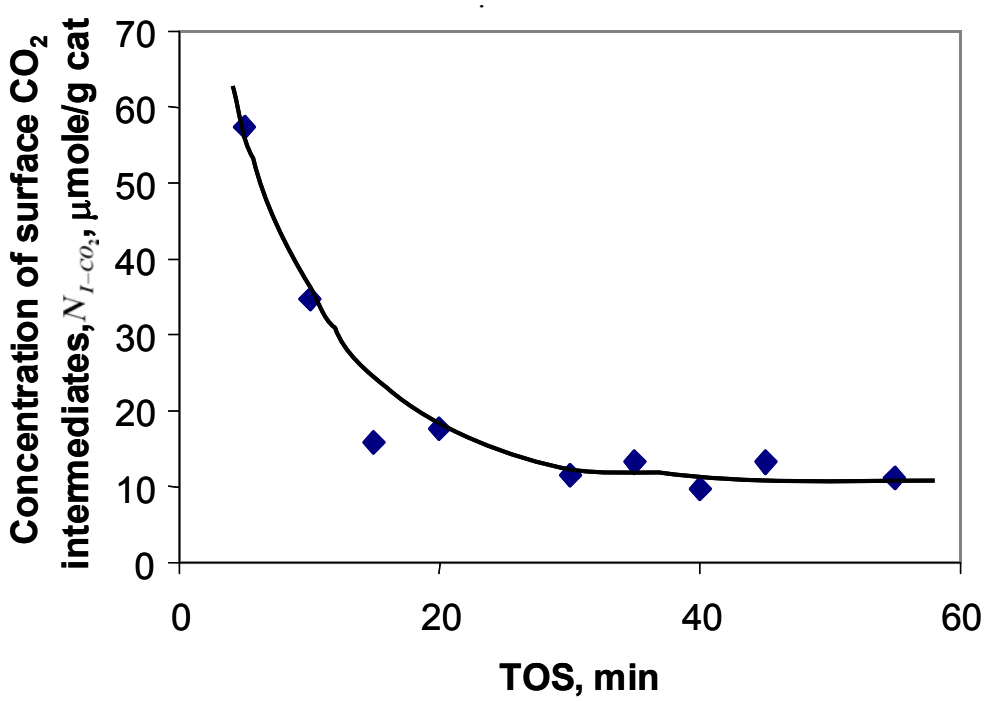
Concentration of surface CO_2 intemediates, N_{I-CO_2}, µmole/g cat
70
60
50
40
30
20
10
0
0
20
40
60
TOS, min

Fig. 9

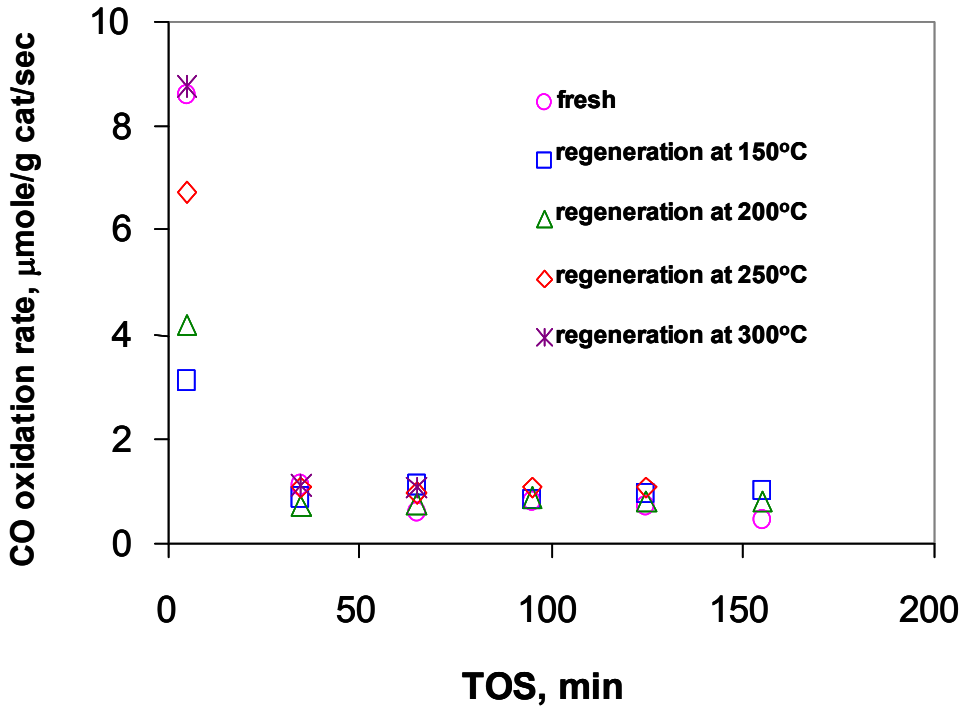
CO oxidation rate, µmole/g cat/sec
10
8
6
4
2
0
0
50
100
150
200
TOS, min
fresh
regeneration at 150°C
regeneration at 200°C
regeneration at 250°C
regeneration at 300°C

Appendix C

Transient (NCSU) Study

CO = 1% , O_2/CO = 1

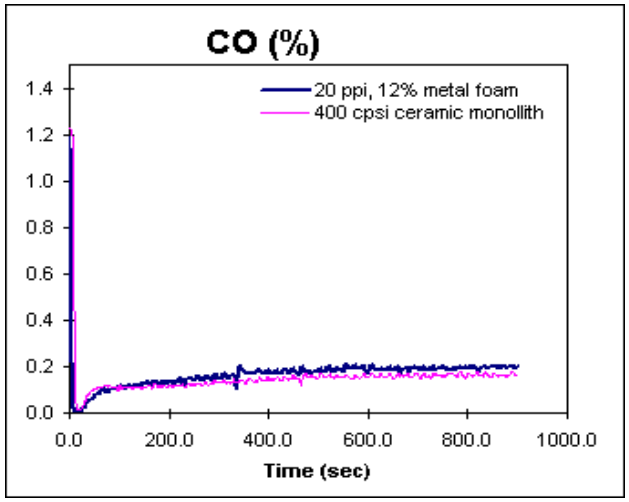
CO (%)
20 ppi, 12% metal foam
400 cpsi ceramic monolith
1.4
1.2
1.0
0.8
0.6
0.4
0.2
0.0
0.0
200.0
400.0
600.0
800.0
1000.0
Time (sec)

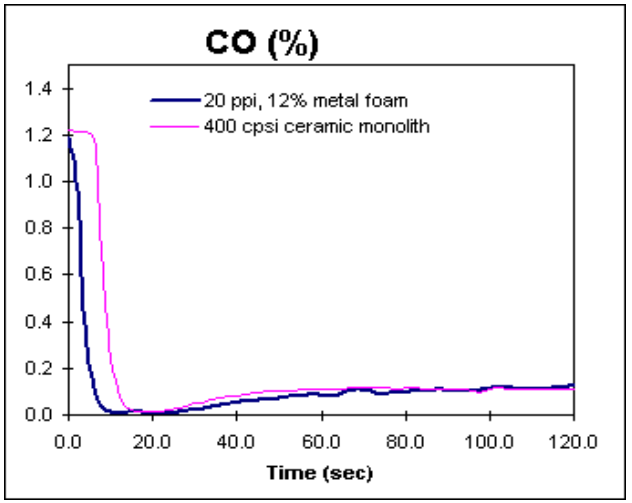
CO (%)
20 ppi, 12% metal foam
400 cpsi ceramic monolith
1.4
1.2
1.0
0.8
0.6
0.4
0.2
0.0
0.0
20.0
40.0
60.0
80.0
100.0
120.0
Time (sec)

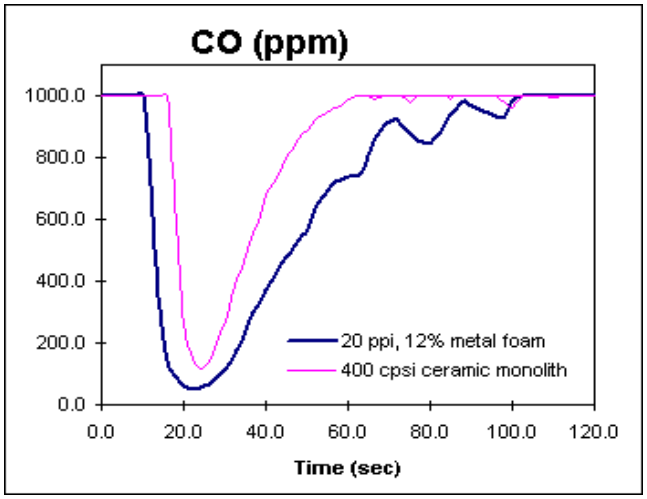
CO (ppm)
1000.0
800.0
600.0
400.0
200.0
0.0
20 ppi, 12% metal foam
400 cpsi ceramic monolith
0.0
20.0
40.0
60.0
80.0
100.0
120.0
Time (sec)

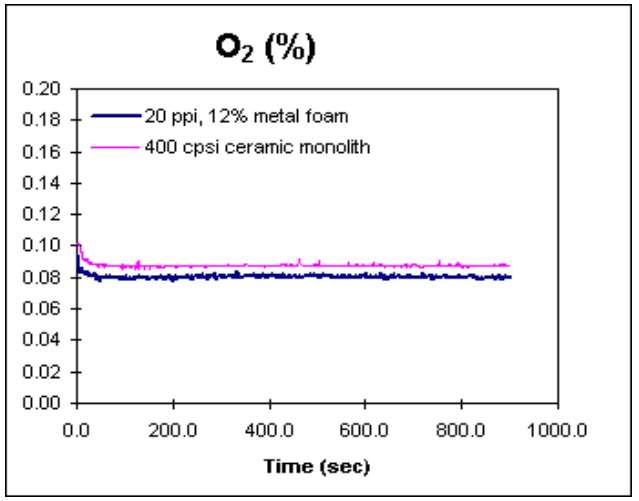
O_2 (%)
0.20
0.18
0.16
0.14
0.12
0.10
0.08
0.06
0.04
0.02
0.00
20 ppi, 12% metal foam
400 cpsi ceramic monolith
0.0
200.0
400.0
600.0
800.0
1000.0
Time (sec)

	Ceramic monolith		20 ppi, 12% density foam	
Time (min)	Tout (°C)			
	O_2/CO = 1	O_2/CO =0.5	O_2/CO = 1	O_2/CO = 0.5
0.0	109	108	109	107
0.5	111	112	113	110
1.0	124	121	136	126
1.5	134	126	155	137
2.0	143	130	164	143
2.5	151	134	172	146
3.0	158	137	178	149
3.5	164	140	184	152
4.0	170	143	189	154
4.5	175	145	193	156
5.0	179	148	197	158
5.5	183	149	200	159
6.0	186	151	203	161
6.5	189	153	206	162
7.0	192	154	208	163
7.5	194	155	210	164
8.0	197	156	212	165
8.5	199	157	214	166
9.0	201	158	216	167
9.5	202	159	218	167
10.0	203	160	219	168
10.5	205	161	220	168
11.0	206	161	221	169
11.5	207	161	222	169
12.0	208	162	223	169
12.5	209	163	224	170
13.0	210	163	225	170
13.5	211	163	225	170
14.0	211	164	226	171
14.5	212	164	227	171
15.0	213	165	227	171

Transient Study:

Record the CO and O_2 concentration and outlet temperature from time zero to the time the reaction reaches steady state.

The preliminary study did not show significant transient difference for metal foam and ceramic monolith support.

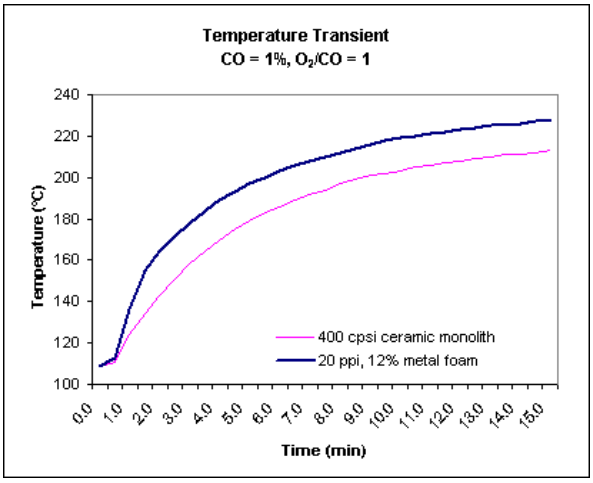

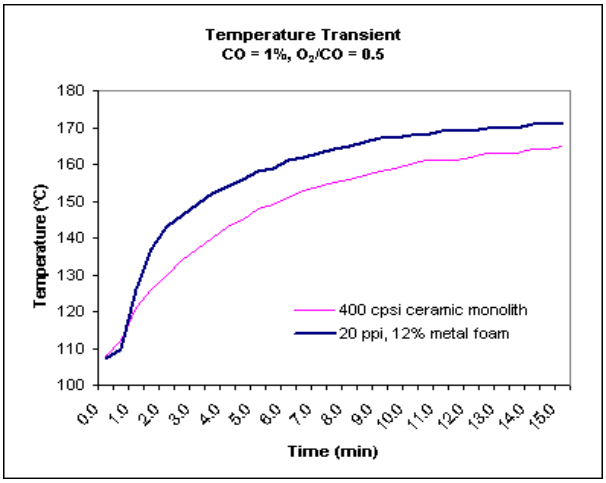

Appendix D

First Order Kinetics Assumption Calculations

Assumptions

(1) First order kinetics $r_{CO} = -k_{CO}[CO]$

(2) Isothermal Reactor conditions k is constant

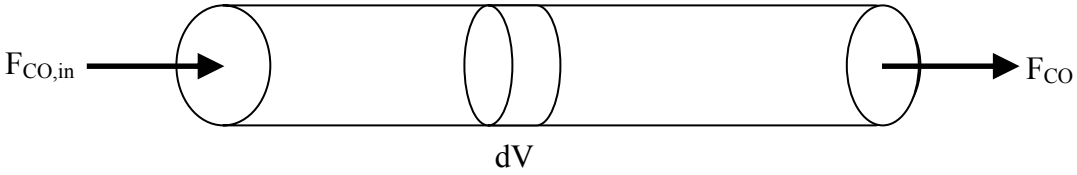

Mass Balance: $F_{CO,in} = \left(F_{CO,in} + dF_{CO}\right) - r_{CO}dV$

$$F_{CO,in} = \left[F_{CO,in} + d\left\{F_{CO,in}\left(1 - X_{CO}\right)\right\}\right] - r_{CO}dV$$

$$F_{CO,in}dX_{CO} = r_{CO}dV$$

$$dF_{CO} = r_{CO}dV \qquad \text{but} \qquad F_{CO} = [CO]\dot{V}_{CO}$$

$$\frac{\dot{V}_{CO}d[CO]}{dV} = -k_{CO}[CO] \qquad \text{but} \qquad \tau = \frac{V}{\dot{V}}$$

$$\frac{d[CO]}{d\tau} = -k_{CO}[CO]$$

$$\int_{[CO]_o}^{[CO]} \frac{d[CO]}{[CO]} = -k_{CO}\int_0^{\tau} d\tau$$

$$\ln\left(\frac{[CO]}{[CO]_o}\right) = -k_{CO}\tau \qquad \text{but} \qquad [CO] = [CO]_o\left(1 - X_{CO}\right)$$

$$\ln\left\{\frac{[CO]_o\left(1 - X_{CO}\right)}{[CO]_o}\right\} = -k_{CO}\tau \qquad \text{but} \qquad \tau = \frac{1}{GHSV}$$

Final Solution:

$$\boxed{\ln\left(1 - X_{CO}\right) = -\frac{k_{CO}}{GHSV}}$$

Nomenclature

$F_{CO,in}$ = Mass flowrate of CO, inlet

F_{CO} = Mass flowrate of CO

dF_{CO} = Differential mass flowrate of CO

$\dot{V}_{CO}$ =Volumetric Flowrate of CO

$[CO]_o$ = initial CO concentration

τ = residence time

r_{CO} = Reaction term for CO

X_{CO} = CO conversion

k_{CO} = CO reaction rate constant

dV = Differential Volume

[CO] = CO concentration

GHSV = Gas Hourly Space Velocity

Appendix E

Individual “Identical” Pieces Data

Comparison of Catalyst Performance for Three "Identical" Metal Foam Pieces

(T_{in} = 150°C, CO inlet = 1.0%, O_2/CO ratio = 1.0, GHSV = 30,000 hr^{-1})

	Xco (%)	Sco (%)	Xo_2 (%)
"Old" Piece	51.3	46.9	104.7
"New" Piece #1	36.9	33.4	105.9
"New" Piece #2	34.5	32.0	103.3

Comparison of Catalyst Performance for Three "Identical" Ceramic Monolith Pieces

(T_{in} = 150°C, CO inlet = 1.0%, O_2/CO ratio = 1.0, GHSV = 30,000 hr^{-1})

	Xco (%)	Sco (%)	Xo_2 (%)
"Old" Piece^{+}	53.3	54.9	96.1
"New" Piece #1	47.2	42.9	105.4
"New" Piece #2	37.7	34.3	105.2

$^{+}$: T_{in} = 170°C

Note: This is the only set operating condition that was tested for all three pieces catalyst, monolith and foam.

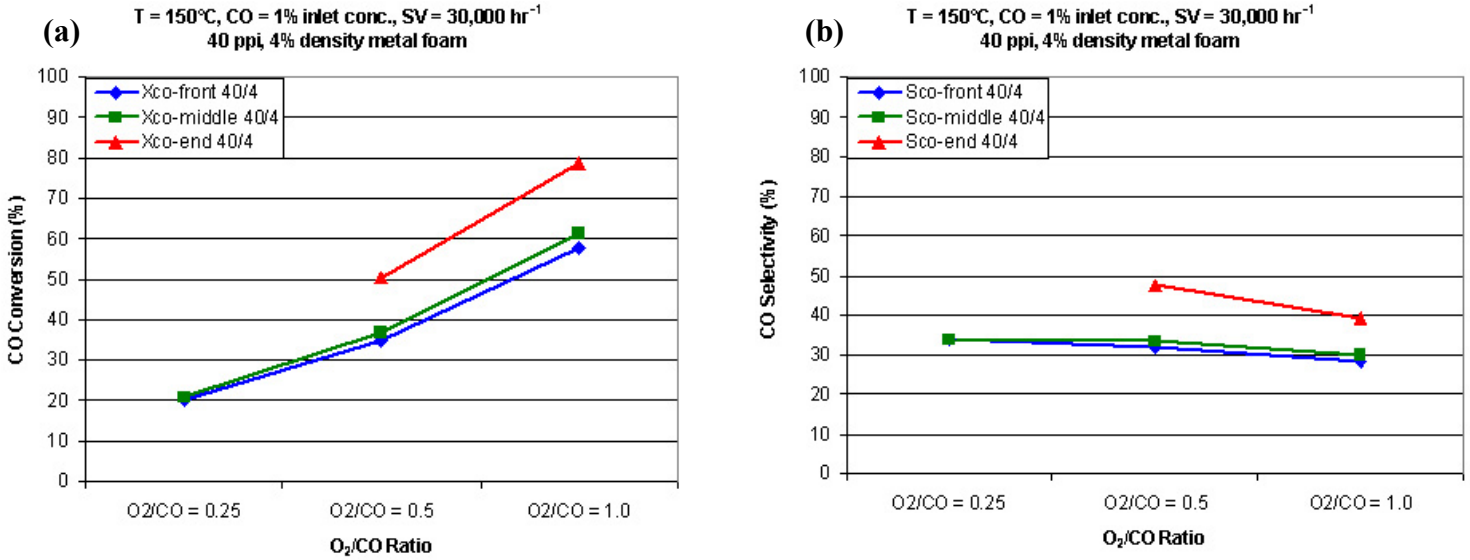

Fig. E1. (a) CO conversion and (b) CO selectivity for three individual "identical" 40 ppi, 4% density metal foams

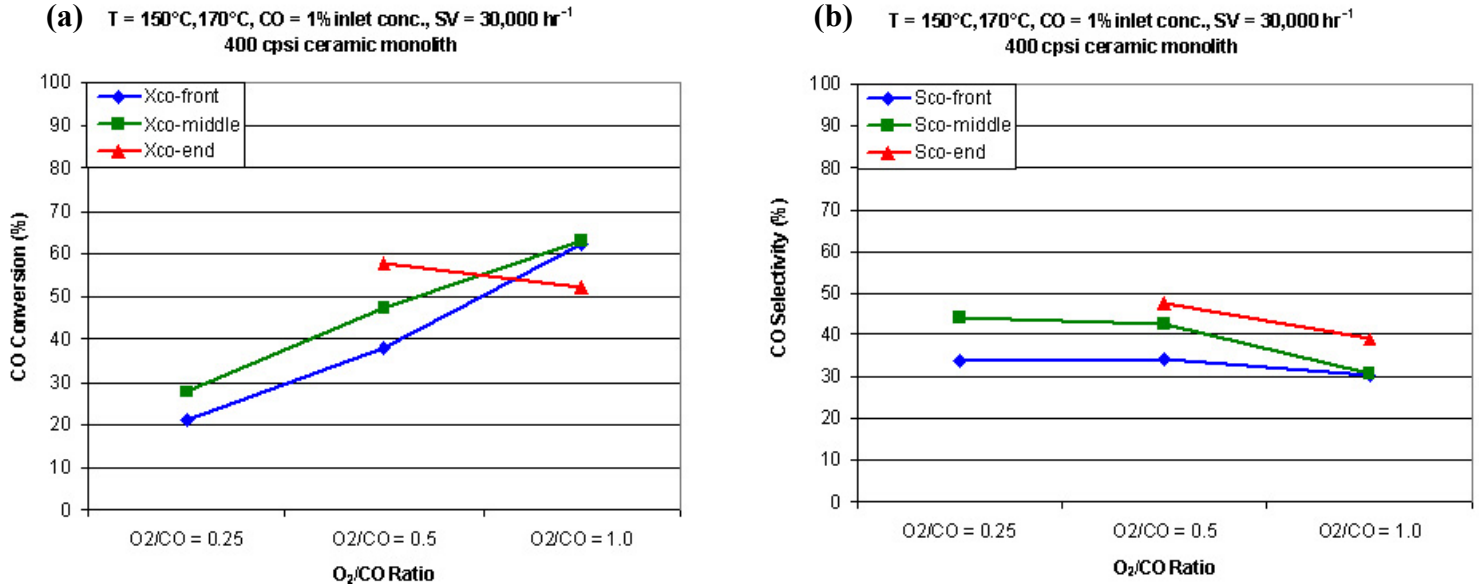

Fig. E2. (a) CO conversion and (b) CO selectivity for three individual "identical" 400 cpsi ceramic monoliths

Appendix F

Comparison of Catalyst Performance for Different Supports

Comparison of Catalyst Performance for Ceramic Foam, Metal Monolith, Metal Foam and Ceramic Monolith

(CO inlet = 1.0%, O_2/CO ratio = 0.5)

		Ceramic Foam 20 ppi, 11% density			**Metal Monolith**			**"new" Metal Foam 40 ppi, 4% density**			**"new" Ceramic Monolith 400 cpsi**		
		Xco(%)	Sco(%)	Xo_2(%)	Xco(%)	Sco(%)	Xo_2(%)	Xco(%)	Sco(%)	Xo_2(%)	Xco(%)	Sco(%)	Xo_2(%)
80°C	30,000 hr^{-1}	4.5	40.2	10.6	20.7	60.4	32.8	50.0	62.2	76.8	36.3	62.3	55.7
	15,000 hr^{-1}	6.3	40.1	15.0	41.8	48.7	82.1	53.5	50.0	103.0	60.8	55.3	105.2
150°C	30,000 hr^{-1}	31.3	35.6	84.1	38.9	35.3	105.6	36.9	33.4	105.9	47.2	42.9	105.4
	45,000 hr^{-1}	22.2	35.5	60.0	40.2	37.5	102.8	39.6	36.2	104.5	50.0	45.4	105.2

Appendix G

ICP/BET Results

Analysis for Kyle bishop and Paul Chin, Chemical Engineering

Prepared By: Wayne P. Robarge

Date: July 28, 2002

Results for Fe and Ni are average of duplicate analyses.

		Projected Composition			Determined Composition			%CV with n = 2		Recovery		
Lab. ID.	Spl. ID.	Pt	Fe	Ni	Pt	Fe	Ni	Fe	Ni	Pt	Fe	Ni
		- % -	- % -	- % -	- % -	- % -	- % -	- % -	- % -	- % -	- % -	- % -
75		5	-	-	4.702	-	-	-	-	94.0	-	-
76		5	2	-	4.482	1.727	-	8.7	-	89.6	86.4	-
77		5	0.5	-	4.558	0.491	-	5.5	-	91.2	98.2	-
78		5	0.05	-	4.740	0.066	-	3.0	-	94.8	132.7	-
79		5	-	0.66	4.403	-	0.621	-	10.4	88.1	-	94.1
80		0.5	0.005	-	0.538	0.015		0.7	-	107.7	302.3	-
81	020000	2	-	-	2.008	-	-	-	-	100.4	-	-
82	020005	2	0.05	-	2.049	0.066	-	13.8	-	102.4	131.7	-
83	020050	2	0.5	-	1.955	0.501	-	7.1	-	97.8	100.3	-
84	005000	0.5	-	-	0.505	-	-	-	-	101.1	-	-
85	005005	0.5	0.05	-	0.527	0.061	-	18.1	-	105.4	121.5	-
86	005050	0.5	0.5	-	0.524	0.550	-	6.8	-	104.8	110.1	-

Digestion Procedure:

Sample Amount: 0.100 - 0.200 grams

React sample with 3 mL of concentrated HF acid in Teflon beaker. Take to dryness.

Add 15 mL of aqua regia and allow to refux on hot plate for 30 - 45 minutes.

Remove from hot plate and allow to cool. Make to vulume in appropriate volumetric flask.

Dissolution of sample matric is essentially complete except for few fine particles in solution.

Elemental analyses were conducted on Perkin-Elmer Model 2000 DV in axial mode.

Comment:

The Fe and Ni analyses are mean of true duplicates - separate samples weighed out and analyzed on separate days. The sample size is very small since the material is dense. It is possible that your material in not that homogeneous. Given the small sample size I use for the analysis, I would need to do a fair number of replicates to get a better idea of the variability in the composition of the material.

BET Results:

NCSU:

Catalysts			BET Surface Area
% Pt	%Fe	% Ni	(m^2/g)
5	0	0	124
5	0.05	0	149
5	0.5	0	133
5	2	0	141
5	0	0.66	106
2	0	0	127
2	0.05	0	129
2	0.5	0	131
0.5	0	0	130
0.5	0.05	0	127
0.5	0.5	0	129

Environex:

Catalysts			BET Surface Area
% Pt	%Fe	% Ni	(m^2/g)
0.5	0.005	0	172

Note: The 5% Pt catalysts were tested last. During these runs I was unable to get consistent readings from the balance. This likely led to the diversity of the results. The 2% Pt and 0.5% Pt catalysts are more representitive of the NCSU catalysts.

BET Theory [7]

$$\frac{p}{n^s\left(p_o - p\right)} = \frac{\left(C-1\right)}{n_m^s C}\frac{p}{p_o} + \frac{1}{n_m^s C}$$

C constant related to the heat of adsorption into the first layer (ΔH_1) and the heat of condensation of the adsorbate (ΔH_c)
n^s quantity of gas adsorbed at an equilibrium pressure
n^s_m the value of n^s at monolayer coverage
p equilibrium pressure
p_o vapour pressure of adsorbate in the condensed state at the adsorption temperature

$$C = R * \exp\left[\frac{\Delta H_c - \Delta H_1}{RT}\right]$$

R constant being approximately j_s/j_c
j_s partition function for the internal degrees of freedom for a molecule in the first adsorbed layer
j_c partition function for the internal degrees of freedom for a molecule in the condensed phase
R Universal Gas Law constant
T adsorption temperature

$$A = a_m n_m^s$$

A surface area of the adsorbent
a_m effective area per molecule in the monolayer